Published February 20, 2012

and essential thrombocythemia, suggested a contribution of *HMGA2* to the development and/or progression of PMF (Guglielmelli et al., 2007). To address this, we evaluated the proliferative and differentiation capacity of *Hmga2*-overexpressing CD34$^-$LSK HSCs. In all experiments, transduction efficiency was ~90% as determined by flow cytometry using GFP as a marker (unpublished data). In liquid cultures supplemented with SCF, TPO, IL-3, IL-6/IL-6 receptor fusion protein (FP6), and EPO, *Hmga2*-overexpressing HSCs showed a growth advantage compared with the control (Fig. 4 A), and the *Hmga2* culture contained significantly more LSK cells than the control at day 10 of culture

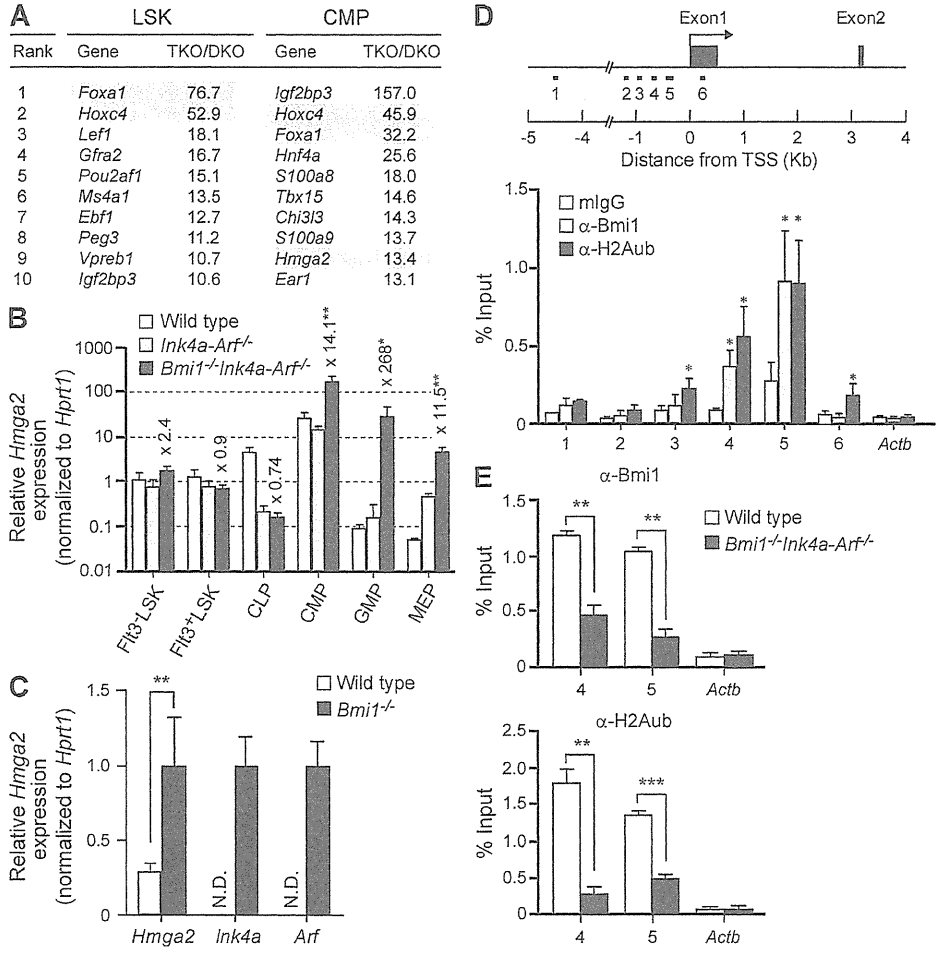

Figure 3. Derepression of *Hmga2* in *Bmi1*$^{-/-}$*Ink4a-Arf*$^{-/-}$ hematopoietic cells. (A) List of top 10 genes up-regulated in LSK cells and CMPs in the absence of Bmi1. IL-7Rα LSK cells purified from BM of 4-wk-old *Ink4a-Arf*$^{-/-}$ (DKO) and *Bmi1*$^{-/-}$*Ink4a-Arf*$^{-/-}$ (TKO) mice and CMPs from recipients' BM at 4 mo after infusion of DKO and TKO BM cells were subjected to microarray analyses and their profiles were compared. Highlighted genes were further characterized in this study. (B) Quantitative RT-PCR analysis of *Hmga2* expression. mRNA levels in each progenitor fraction from the recipients' BM repopulated by BM cells of the indicated genotype at 4 mo after transplantation were normalized to *Hprt1* expression. Expression levels relative to those in the wild-type Flt3$^-$ LSK cells are shown as the mean ± SD for triplicate analyses. The fold change in expression levels between *Bmi1*$^{-/-}$*Ink4a-Arf*$^{-/-}$ cells and *Ink4a-Arf*$^{-/-}$ cells is also indicated. *, $P < 0.05$; **, $P < 0.01$. (C) Derepression of *Hmga2* in *Bmi1*-deficient hematopoietic cells. Lineage$^-$c-Kit$^+$ cells were purified from BM of 4-wk-old wild-type and *Bmi1*$^{-/-}$ mice. mRNA levels of *Hmga2*, *Ink4a*, and *Arf* were normalized to *Hprt1* expression. Expression levels relative to those in the *Bmi1*$^{-/-}$ cells are shown as the mean ± SD for triplicate analyses. N.D. indicates not detected. **, $P < 0.01$. (D) ChIP analysis at the *Hmga2* promoter in wild-type Lineage$^-$c-Kit$^+$ cells. The *Hmga2* locus indicating its genomic structure (based on the Ensemble data, transcript ID ENSMUST00000072777) is depicted in the top panel. Exons are demarcated by black boxes. The regions 1–6 amplified from the precipitated DNA by site-specific quantitative PCR are indicated. The binding of Bmi1 and the levels of H2Aub were determined by ChIP using control mouse IgG (mIgG), anti-Bmi1, and anti-H2Aub antibodies and site-specific real-time PCR. The relative amount of immunoprecipitated DNA is presented as a percentage of input DNA (bottom). The data are shown as the mean ± SD for four independent experiments. The β-*actin* promoter (*Actb*) served as a negative control. *, $P < 0.05$. (E) ChIP analysis at the *Hmga2* promoter in wild-type or *Bmi1*$^{-/-}$*Ink4a-Arf*$^{-/-}$ Lineage$^-$ cells. The binding of Bmi1 and the levels of H2Aub were determined by ChIP using anti-Bmi1 or anti-H2Aub antibodies and site-specific real-time PCR as in D. The data are shown as the mean ± SD for triplicate PCRs from two independent experiments. *, $P < 0.05$; **, $P < 0.01$; ***, $P < 0.001$.

Published February 20, 2012

(Fig. 4 B). Morphological analysis unveiled a drastic enhancement in production of megakaryocytes upon the overexpression of *Hmga2*. The *Hmga2* culture contained significantly more multinucleated megakaryocytes and mononuclear micromegakaryocytes (Fig. 4, C and D).

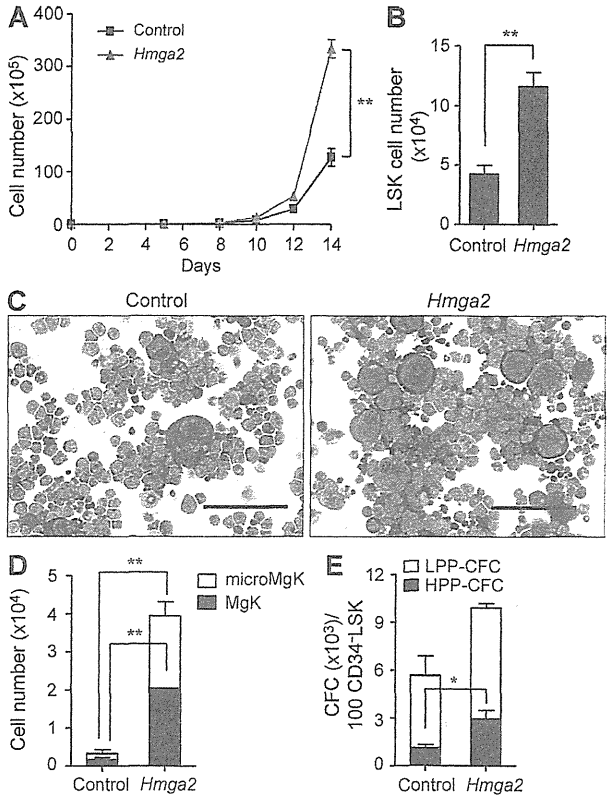

Figure 4. *Hmga2* promotes expansion of progenitor cells and enhances megakaryocytopoiesis in vitro. (A) Growth of CD34$^-$LSK HSCs transduced with the *Hmga2* retrovirus. 100 CD34$^-$LSK HSCs were transduced with either the empty vector or *Hmga2* retrovirus and cultured in the presence of SCF, TPO, IL-3, FP6, and EPO for 14 d. Numbers of cells are shown as the mean ± SD for triplicate cultures. **, $P < 0.01$. (B) Number of LSK cells in culture. Flow cytometric analysis of the culture in A was performed at day 10 of culture. Absolute numbers of LSK cells are indicated as the mean ± SD ($n = 3$). **, $P < 0.01$. (C) Morphology of CD34$^-$LSK HSCs at day 12 of culture. CD34$^-$LSK HSCs transduced with the indicated retroviruses in A were recovered, cytospun onto slide glasses, and subjected to May-Grünwald Giemsa staining. The morphology of the cells was observed under a light microscope. Bars, 100 µm. (D) The frequency of multinucleated megakaryocytes (MgK) and mononuclear micromegakaryocytes (microMgK) in culture. The cytospun cells on slide glasses in C were examined under a light microscope and absolute numbers in culture are indicated as the mean ± SD. Counts of 500 cells were independently performed three times. **, $P < 0.01$. (E) Effect of *Hmga2* on CFC numbers in culture. 100 CD34$^-$LSK HSCs were transduced with the indicated retrovirus and cultured in the presence of SCF and TPO. At day 10 of culture, colony assays were performed to evaluate the number of CFCs in culture. Absolute numbers of low proliferative potential (LPP; diameter <1 mm) and HPP (diameter ≥1 mm) CFCs are shown as the mean ± SD for triplicate cultures. *, $P < 0.05$; **, $P < 0.01$.

We then cultured transduced HSCs for 9 d (10 d of culture in total) in the presence of SCF and TPO, which supports the proliferation of HSCs and progenitors rather than their differentiation (Ema et al., 2000). The total number of colony-forming cells (CFCs) was significantly increased in the *Hmga2* culture (Fig. 4 E). Among CFCs, the number of high proliferative potential (HPP)-CFCs, which generate a colony with a diameter >1 mm, was increased with *Hmga2* compared with the control. These results indicate that overexpression of *Hmga2* promotes expansion of progenitor cells and also facilitates the proliferation and differentiation of megakaryocytic cells in vitro.

Forced expression of *Hmga2* promotes megakaryocytopoiesis and induces myeloproliferative hematopoiesis in vivo

We next examined the effect of *Hmga2* overexpression on hematopoiesis in vivo. We performed competitive repopulation assays using 30 CD34$^-$LSK HSCs transduced with *Hmga2* (CD45.2) at day 3.5 of culture along with 2×10^5 fresh unfractionated BM cells (CD45.1) for radioprotection. *Hmga2*-overexpressing cells showed a greater, albeit not statistically significant, contribution to the myeloid lineage in peripheral blood (PB) compared with the control (Fig. 5 A). Recipients repopulated with *Hmga2*-overexpressing cells had significantly more LSK cells and myeloid progenitors in BM compared with the control (Fig. 5 C). Furthermore, they also had mild splenomegaly with extramedullary hematopoiesis as evident from a marginal increase in LSK HSCs/MPPs in the spleen and a significant increase in the PB (Fig. 5 B and C). The recipients repopulated with *Hmga2*-overexpressing cells appeared to have more megakaryocytes in the BM (not depicted) and platelets in the PB (Fig. 5 D). These findings indicate that derepression of *Hmga2* could induce an MPN-like state with enhanced megakaryocytopoiesis and correspond well with findings recently obtained with transgenic mice carrying a 3′-UTR–truncated *Hmga2* cDNA (Δ*Hmga2* mice; Ikeda et al., 2011). Δ*Hmga2* mice developed MPN-like hematopoiesis with an increased number of megakaryocytes in the BM, although the number of platelets in the PB was not described. Together, these findings implicate *Hmga2* in the PMF-like pathological hematopoiesis induced by *Bmi1*$^{-/-}$ *Ink4a-Arf*$^{-/-}$ BM cells.

Given that *HMGA2* is highly derepressed in CD34$^+$ stem and progenitor cells in PMF patients, PcG function could be compromised in PMF patients, partly by loss-of-function mutations of *EZH2*. Indeed, we confirmed that Ezh2 also regulates *Hmga2* as Bmi1 does. *Hmga2* was highly derepressed in *Ezh2*-deficient progenitor cells (unpublished data). ChIP assays demonstrated that the *Hmga2* promoter is bound by Ezh2 and marked with H3K27me3 in wild-type BM Lineage$^-$c-Kit$^+$ progenitors (unpublished data). Interestingly, recipient mice repopulated with *Ezh2*-deficient BM cells showed an increase in the platelet count in PB similar to recipients repopulated with HSCs overexpressing *Hmga2* (Mochizuki-Kashio et al., 2011). These data indicate that both *Bmi1* and *Ezh2* transcriptionally repress *Hmga2*. However, the

Published February 20, 2012

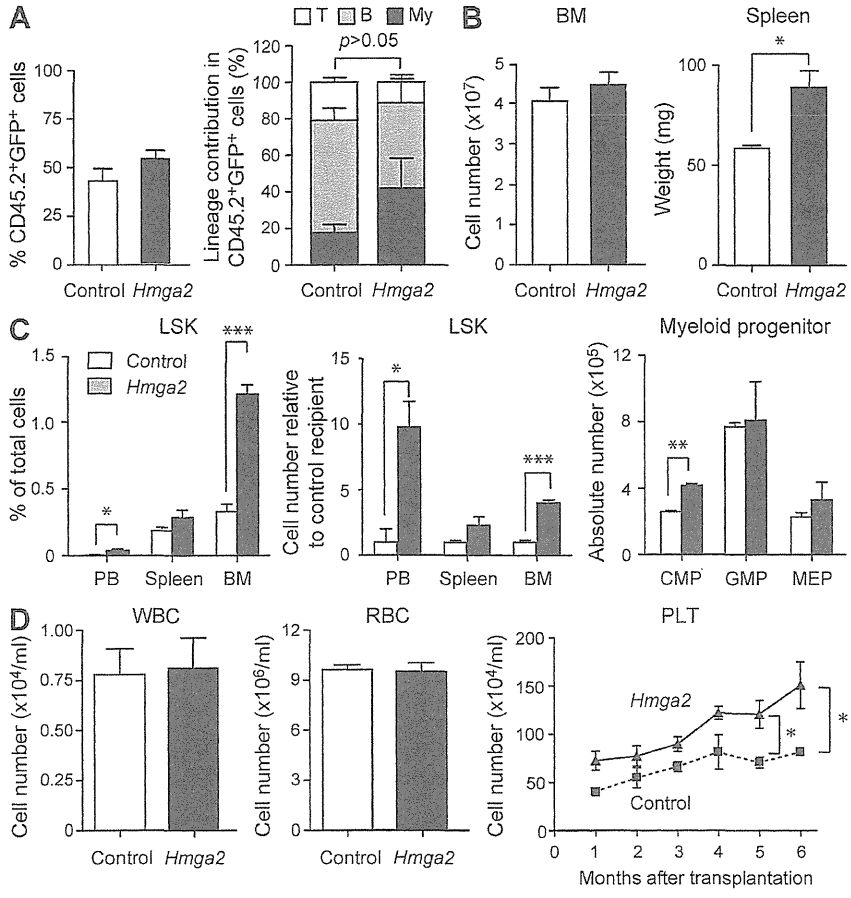

Figure 5. Forced expression of *Hmga2* causes myeloproliferative hematopoiesis with enhanced megakaryocytopoiesis. (A) Donor chimerism and lineage contribution in PB ($n = 5$). CD34$^-$LSK HSCs (CD45.2) transduced with either control or *Hmga2* retrovirus were transplanted into lethally irradiated CD45.1 mice together with 2×10^5 BM competitor cells from 8-wk-old CD45.1 mice. The chimerism of CD45.2$^+$GFP$^+$-transduced cells in PB of recipient mice was examined at 6 mo after transplantation (left). Lineage contribution of CD45.2$^+$GFP$^+$ donor cells to myeloid (Gr-1$^+$ and/or Mac-1$^+$), B (B220$^+$), or T (CD4$^+$ or CD8$^+$) cells (right). Data are presented as the mean ± SD ($n = 6$). (B) Absolute numbers of BM mononuclear cells (from bilateral femurs and tibiae) and spleen weights at 6 mo after transplantation. Data are presented as the mean ± SD ($n = 6$). *, $P < 0.05$. (C) Frequency of LSK cells and absolute numbers of myeloid progenitor cells in BM. The frequency of LSK cells in PB, BM, and spleen (left) and absolute numbers of myeloid progenitor cells in BM (right) of recipient mice examined 6 mo after transplantation. The relative number of LSK cells is presented in the middle panel. Data are presented as the mean ± SD ($n = 6$). *, $P < 0.05$; **, $P < 0.01$; ***, $P < 0.001$. (D) PB cell counts of recipients repopulated with CD34$^-$LSK HSCs transduced with the indicated retrovirus. Cell counts at 6 mo after transplantation are presented for white blood cells (WBC) and red blood cells (RBC). The time course of the increase in platelet (PLT) counts is also depicted. Data are presented as the mean ± SD ($n = 6$). *, $P < 0.05$.

frequency of *EZH2* mutations in PMF has been reported to be only 13% (Nikoloski et al., 2010). Thus, it would be intriguing to examine other mechanisms that compromise PcG function in PMF patients without *EZH2* mutations.

Nevertheless, it should be noted that *Hmga2* is not the only oncogenic target of Bmi1 responsible for the establishment of PMF-like disease, as fibrosis was not seen in recipient BM that was repopulated with *Hmga2*-overexpressing cells at 6 mo after transplantation (unpublished data). As evident from the significant increase in platelet counts, overexpression of *Hmga2* does not compromise the terminal differentiation of megakaryocytes. It has been proposed that necrotic megakaryocytes in BM are the main causative factor for myelofibrosis. Although derepression of *Hmga2* induces an MPN-like state with enhanced megakaryocytopoiesis, it may require the derepression of other Bmi1 targets to eventually induce a fibrotic state after a preceding MPN-like state. Our microarray analysis also identified *Hoxc4* and *Foxa1* as being derepressed in *Bmi1*$^{-/-}$*Ink4a-Arf*$^{-/-}$ cells (Fig. 3 A). We confirmed this derepression by RT-PCR (unpublished data), and *Hoxc4* and *Foxa1* also appeared to be direct targets of Bmi1 by ChIP assays (unpublished data). We tested the effects of forced expression of these genes in HSCs, but failed to induce an MPN-like disease in recipient mice (unpublished data).

Collectively, our findings indicate that *Bmi1* antagonizes the development of MPN in the absence of its major tumor-suppressive targets, *Ink4a* and *Arf*, and we showed the tumor suppressive function of Bmi1 through epigenetic silencing of oncogenes. Although *Bmi1*-deficiency is self-limiting unless *Ink4a* and *Arf* are deleted first, *INK4A* and *ARF* are frequently inactivated by deletions or mutations, or transcriptionally repressed by DNA methylation at their promoters in human cancers. Therefore, the situations like the *Ink4a/Arf*-null background that we used in this study also happen in the initiation and progression of human cancers. Our findings suggest that in such situations, the tumor cells with impaired BMI1 function could outcompete cells with normal BMI1 function because the effects of derepressed oncogenes, such as *HMGA2*, appear to supersede the effects of derepressed tumor suppressor genes. Corresponding to our findings, PRC1 has been reported to exert tumor suppressor activity through epigenetic silencing of Notch and JAK-STAT signaling in *Drosophila melanogaster* eyes (Martinez et al., 2009; Classen et al., 2009). Furthermore, mice with hypomorphic mutations of *Eed* and *Suz12* show enhanced hematopoiesis (Lessard et al., 1999; Majewski et al., 2008). All of these findings support the

Published February 20, 2012

tumor suppressor function of EZH2 observed in human myelodysplastic syndrome and MPN, and are suggestive of a broad range of target genes of the PcG proteins, including both oncogenes and tumor suppressor genes. Although tumor suppressor genes have been stressed as PcG targets, our findings shed light on the role of PcG proteins in the gene silencing of oncogenes. Thus, the PcG proteins fine-tune the growth of hematopoietic cells in both a positive and a negative manner to maintain hematopoietic homeostasis.

MATERIALS AND METHODS

Mice. *Bmi1*$^{+/-}$ mice (van der Lugt et al., 1994) and *Ink4a-Arf*$^{-/-}$ mice (Serrano et al., 1996) that had been backcrossed at least eight times onto a C57BL/6 (CD45.2) background were used. C57BL/6 (CD45.2) mice and C57BL/6 mice congenic for the Ly5 locus (CD45.1) were purchased from Japan SLC and Sankyo Laboratory Service, respectively. Littermates were used as controls in all experiments. All mice were bred and maintained in the Animal Research Facility of the Graduate School of Medicine, Chiba University in accordance with institutional guidelines. All experiments using mice received approval from the Chiba University Administrative Panel for Animal Care.

Competitive repopulation assay. BM cells (10^6) from 4-wk-old CD45.2 mice were mixed with the same number of unfractionated BM competitor cells (CD45.1) and transplanted into CD45.1 mice irradiated at a dose of 9.5 Gy. PB cells of the recipient mice were analyzed with a mixture of antibodies that included PE-Cy7–conjugated anti-CD45.1, Pacific blue–conjugated anti-CD45.2, PE-conjugated anti–Mac-1 and anti–Gr-1, APC-conjugated anti-B220, and APC-Cy7–conjugated anti-CD4 and anti-CD8α antibodies. Cells were analyzed on a FACSCanto II (BD). Donor cell chimerism in the recipient PB cells was evaluated as percent donor chimerism calculated as (percent donor cells) × 100/(percent donor cells + percent recipient cells). PB cell counts were made using an automated cell counter (Celltec α; Nihon Kohden).

Purification of mouse HSCs and progenitors. Mouse HSCs ($CD34^-LSK$ cells) were purified from BM of 8-wk-old mice. Mononuclear cells were isolated on Ficoll-Paque PLUS (GE Healthcare). The cells were stained with an antibody cocktail consisting of biotinylated anti–Gr-1, Mac-1, IL-7Rα, B220, CD4, CD8α, and Ter119 monoclonal antibodies. $Lineage^+$ cells were depleted with goat anti–rat IgG microbeads (Miltenyi Biotec) through an LD column (Miltenyi Biotec). The cells were further stained with FITC-conjugated anti-CD34, PE-conjugated anti–Sca-1, and APC-conjugated anti–c-Kit antibodies. Biotinylated antibodies were detected with APC-Cy7–conjugated streptavidin. Analysis and sorting were performed on a FACS Aria II (BD). CMPs, GMPs, MEPs, and CLPs were analyzed as $CD34^+FcγR^{low}c\text{-}Kit^+Sca\text{-}1^-Lineage^-IL\text{-}7Rα^-$ cells, $CD34^+FcγR^{hi}c\text{-}Kit^+Sca\text{-}1^-Lineage^-IL\text{-}7Rα^-$ cells, $CD34^-FcγR^{low}c\text{-}Kit^+Sca\text{-}1^-Lineage^-IL\text{-}7Rα^-$ cells, and $IL\text{-}7Rα^+c\text{-}Kit^{low}Sca\text{-}1^{low}Lineage^-$ cells, respectively.

Retroviral vectors expressing *Hmga2* and virus production. Full-length mouse *Hmga2* cDNA in the pMY-ires-EGFP retroviral expression vector was kindly provided by K. Nakashima (Nara Institute of Science and Technology, Ikoma, Nara, Japan). A recombinant vesicular stomatitis virus glycoprotein (VSV-G)-pseudotyped high-titer retrovirus was generated by a 293gpg packaging cell line that had been engineered to express the VSV-G protein under the control of a tetracycline-inducible system. The virus in supernatants of 293gpg cells was concentrated by centrifugation at 6,000 *g* for 16 h. Viral titers were determined by infecting Jurkat cells (a human T cell line).

Transduction of $CD34^-LSK$ HSCs. $CD34^-LSK$ HSCs were transduced with the indicated retrovirus, as previously described, with minor modifications (Iwama et al., 2004). $CD34^-LSK$ HSCs were sorted into 96-well microtiter plates coated with the recombinant human fibronectin fragment CH-296 (RetroNectin; Takara Shuzo) at 100 cells per well, and then incubated in α-MEM supplemented with 1% FBS, 1% L-glutamine, penicillin, streptomycin solution (GPS; Sigma-Aldrich), 50 μM 2-mercaptoethanol (2-ME), 100 ng/ml mouse stem cell factor (SCF; PeproTech), and 100 ng/ml human thrombopoietin (TPO; PeproTech) for 24 h. Next, cells were transduced with the indicated retrovirus at a multiplicity of infection (MOI) of 1,500 in the presence of 1 μg/ml RetroNectin and 10 μg/ml protamine sulfate (Sigma-Aldrich) for 24 h. After transduction, cells were further incubated in the same medium for 9 d, subjected to in vitro colony assays or in S-Clone SF-O3 (Sanko Junyaku) supplemented with 0.2% BSA, 50 μM 2-ME, 1% GPS, 50 ng/ml SCF, and 50 ng/ml TPO for 2.5 d, and then subjected to competitive repopulation assays. The transduction efficiency was nearly 90%, as judged from GFP expression. Colony assays were performed using a methylcellulose medium (M3234; STEMCELL Technologies) supplemented with 20 ng/ml mouse SCF, 20 ng/ml mouse IL-3 (PeproTech), 50 ng/ml human TPO, and 3 U/ml human EPO (provided by Kyowa Hakko Kirin). Colony numbers were counted on day 10. $CD34^-LSK$ HSCs (CD45.2) transduced with the indicated retrovirus were also transplanted intravenously into 8-wk-old CD45.1 mice irradiated at a dose of 9.5 Gy, together with 2×10^5 BM competitor cells from 8-wk-old CD45.1 mice.

Microarray analysis. $IL\text{-}7Rα^-LSK$ cells were purified from BM of 4-wk-old *Ink4a-Arf*$^{-/-}$ and *Bmi1*$^{-/-}$*Ink4a-Arf*$^{-/-}$ mice and CMPs from recipients' BM at 4 mo after infusion of *Ink4a-Arf*$^{-/-}$ or *Bmi1*$^{-/-}$*Ink4a-Arf*$^{-/-}$ BM cells. Total RNA was isolated using TRIZOL LS Reagent (Invitrogen), and its integrity was confirmed using LabChip RNA 6000 Nano chips and a 2100 Bioanalyzer (Agilent Technologies). Target cRNA was prepared from the total RNA equivalent to 10,000 cells ($IL\text{-}7Rα^-$ LSK) or 8,000 cells (CMPs) with a two-cycle cDNA synthesis kit and 3′-amplification reagents for IVT labeling (Affymetrix), and then hybridized to a GeneChip Mouse Genome 430 2.0 oligonucleotide microarray (Affymetrix) according to the manufacturer's instructions. The expression value of each gene was calculated and normalized using GeneChip Operating Software version 1.4 (Affymetrix). All data are MIAME compliant, and the raw data were deposited in Gene Expression Omnibus (accession no. GSE19796 and GSE31086).

Quantitative reverse transcription (RT) PCR analysis. Total RNA was isolated using TRIZOL LS solution (Invitrogen) and reverse transcribed by the ThermoScript RT-PCR system (Invitrogen) with an oligo dT primer. Real-time quantitative PCR was performed with an ABI prism 7300 Thermal Cycler (Applied Biosystems) using FastStart Universal Probe Master (Roche). *Hypoxanthine-guanosine phosphoribosyl transferase 1* (*Hprt1*) expression was used to calculate relative expression levels. The combination of primer sequences and probe numbers are as follows: *Hmga2*, probe #26, 5′-AAGGCAGCAAAAACAAGAGC-3′ and 5′-CCGTTTTTCTCCAATGGTCT-3′; *Hprt1*, probe #95, 5′-TCCTCCTCAGACCGCTTTT-3′ and 5′-CCTGGTTCATCATCGCTAATC-3′.

ChIP assay. $Lineage^-$ or $Lineage^-c\text{-}Kit^+$ BM cells (2×10^5 cells/antibody) isolated by flow cytometry were cross-linked with 1% formaldehyde for 15 min at room temperature, and incubated for 5 min at 4°C after the addition of 0.125 M glycine. Cells were washed with PBS, lysed with cell lysis buffer (50 mM Tris-HCl, pH 8.0, 10 mM EDTA, 150 mM NaCl, 0.5% SDS, and protease inhibitor cocktail [PIC; Roche]) on ice, and sonicated until the DNA fragments were 200–500 bp in mean size as measured by Bioruptor (Cosmo Bio). After centrifugation at 15,000 rpm for 10 min, sheared chromatin was diluted 10-fold in dilution buffer (50 mM Tris-HCl, pH 8.0, 150 mM NaCl, 1.1% Triton X-100, 0.11% sodium deoxycholate, and PIC), and precleared by addition of Dynabeads Protein G (Invitrogen) for 1 h at 4°C. For anti-Bmi1 (clone 8A9; provided by N. Nozaki, MAB Institute, Yokosuka, Kanagawa, Japan), precleared chromatin was immunoprecipitated overnight at 4°C with antibody/Dynabeads Protein G mix. For anti–ubiquityl-Histone H2A (H2Aub; clone E6C5, 05–678; Millipore), precleared chromatin was immunoprecipitated overnight at 4°C with anti-H2Aub, followed by the

Published February 20, 2012

addition of anti-mouse IgMμ (12–488; Millipore)/Dynabeads Protein G mix and incubation for 2 h at 4°C. Beads were then sequentially washed with the following combination of wash buffers; twice each with low-salt wash buffer (50 mM Tris-HCl, pH 8.0, 150 mM NaCl, 1 mM EDTA, 1% Triton X-100, 0.1% SDS, and 0.1% sodium deoxycholate), high-salt wash buffer (50 mM Tris-HCl, pH 8.0, 500 mM NaCl, 1 mM EDTA, 1% Triton X-100, 0.1% SDS, and 0.1% sodium deoxycholate), and LiCl wash buffer (10 mM Tris-HCl, pH 8.0, 250 mM LiCl, 1 mM EDTA, 0.5% NP-40, and 0.5% sodium deoxycholate). Bound chromatin was eluted and, together with input DNA, cross-linking was reversed in elution buffer (50 mM Tris-HCl, pH 8.0, 10 mM EDTA, and 1% SDS) by overnight incubation at 65°C. Immunoprecipitated DNA and input DNA were treated with RNaseA (Sigma-Aldrich) and proteinase K (Roche), and extracted with phenol:chloroform. Quantitative PCR analysis was performed using SYBR Premix Ex Taq II (Takara Bio), and the 7500/7500 Fast Real-Time PCR system (Applied Biosystems). Primer sequences are as follows: *Hmga2*, region 1, 5′-GGGAAGCCAGCAGAGGTAAGCC-3′ and 5′-CGAGCGCATTTGCACGGCTC-3′; region 2, 5′-CTGGCACCATCGTGTGTCTGG-3′ and 5′-TGCGCGCACACACACTTCACT-3′; region 3, 5′-GGTCGCTCTTTTCCCGGGGC-3′ and 5′-TCCACCGAGGGTTGCCCG-3′; region 4, 5′-GCCGCCTTCGAGGCAGTTGT-3′ and 5′-CAAGAGGAGGGGGCAGGCCA-3′; region 5, 5′-AAAACTTGGGCTCCGGGTGCAGA-3′ and 5′-GGGCGCCCAGCTCAGCTCTAG-3′; region 6, 5′-CGCTGGACGTCCGGTGTTGAT-3′ and 5′-AAGAGCGGCGAGAGCAGGCG-3′; *Actb*, 5′-CCCAACACACCTAGCAAATTAGAACCAC-3′ and 5′-CCTGGATTGAATGGACAGAGAGTCACT-3′.

Immunofluorescence staining of spleen. Frozen spleen sections were prepared and immunostained according to the method described by Kawamoto (2003). After fixation with 100% ethanol-dry ice and blocking in MAXblock medium (Active Motif) for 1 h at room temperature, spleen sections were incubated with an FITC-conjugated anti-CD41 antibody (BD) for 12 h at 4°C. Spleen sections were then washed and incubated with the DNA marker DAPI for 5 min at room temperature.

We thank M. van Lohuizen and R.A. DePinho for providing *Bmi1*$^{+/-}$ mice and *Ink4a-Arf*$^{-/-}$ mice, respectively, N. Nozaki, K. Helin, T. Kitamura, and K. Nakashima for the anti-Bmi1 antibody (8A9), the anti-Ezh2 antibody (AC22), the pMYs-ires-EGFP vector, and the *Hmga2* cDNA, respectively, and George Wendt for critical reading of the manuscript.

This work was supported in part by Grants-in-aid for Scientific Research (#21390289) and for the Global COE Program (Global Center for Education and Research in Immune System Regulation and Treatment), MEXT, Japan, a Grant-in-aid for Core Research for Evolutional Science and Technology (CREST) from the Japan Science and Technology Corporation (JST), and grants from the Takeda Science Foundation, Astellas Foundation for Research on Metabolic Disorders, and the Tokyo Biochemical Research Foundation. H. Oguro was supported by a postdoctoral fellowship from the Japanese Society for the Promotion of Science.

The authors have no conflicting financial interests.

Submitted: 12 August 2011
Accepted: 27 January 2012

REFERENCES

Andrieux, J., J.L. Demory, B. Dupriez, S. Quief, I. Plantier, C. Roumier, F. Bauters, J.L. Laï, and J.P. Kerckaert. 2004. Dysregulation and overexpression of HMGA2 in myelofibrosis with myeloid metaplasia. *Genes Chromosomes Cancer.* 39:82–87. http://dx.doi.org/10.1002/gcc.10297

Classen, A.K., B.D. Bunker, K.F. Harvey, T. Vaccari, and D. Bilder. 2009. A tumor suppressor activity of Drosophila Polycomb genes mediated by JAK-STAT signaling. *Nat. Genet.* 41:1150–1155. http://dx.doi.org/10.1038/ng.445

Ema, H., H. Takano, K. Sudo, and H. Nakauchi. 2000. In vitro self-renewal division of hematopoietic stem cells. *J. Exp. Med.* 192:1281–1288. http://dx.doi.org/10.1084/jem.192.9.1281

Ernst, T., A.J. Chase, J. Score, C.E. Hidalgo-Curtis, C. Bryant, A.V. Jones, K. Waghorn, K. Zoi, F.M. Ross, A. Reiter, et al. 2010. Inactivating mutations of the histone methyltransferase gene EZH2 in myeloid disorders. *Nat. Genet.* 42:722–726. http://dx.doi.org/10.1038/ng.621

Fusco, A., and M. Fedele. 2007. Roles of HMGA proteins in cancer. *Nat. Rev. Cancer.* 7:899–910. http://dx.doi.org/10.1038/nrc2271

Guglielmelli, P., R. Zini, C. Bogani, S. Salati, A. Pancrazzi, E. Bianchi, F. Mannelli, S. Ferrari, M.C. Le Bousse-Kerdilès, A. Bosi, et al. 2007. Molecular profiling of CD34$^+$ cells in idiopathic myelofibrosis identifies a set of disease-associated genes and reveals the clinical significance of Wilms' tumor gene 1 (WT1). *Stem Cells.* 25:165–173. http://dx.doi.org/10.1634/stemcells.2006-0351

Ikeda, K., P.J. Mason, and M. Bessler. 2011. 3'UTR-truncated Hmga2 cDNA causes MPN-like hematopoiesis by conferring a clonal growth advantage at the level of HSC in mice. *Blood.* 117:5860–5869. http://dx.doi.org/10.1182/blood-2011-02-334425

Iwama, A., H. Oguro, M. Negishi, Y. Kato, Y. Morita, H. Tsukui, H. Ema, T. Kamijo, Y. Katoh-Fukui, H. Koseki, et al. 2004. Enhanced self-renewal of hematopoietic stem cells mediated by the polycomb gene product Bmi-1. *Immunity.* 21:843–851. http://dx.doi.org/10.1016/j.immuni.2004.11.004

Kawamoto, T. 2003. Use of a new adhesive film for the preparation of multi-purpose fresh-frozen sections from hard tissues, whole-animals, insects and plants. *Arch. Histol. Cytol.* 66:123–143. http://dx.doi.org/10.1679/aohc.66.123

Konuma, T., H. Oguro, and A. Iwama. 2010. Role of the polycomb group proteins in hematopoietic stem cells. *Dev. Growth Differ.* 52:505–516. http://dx.doi.org/10.1111/j.1440-169X.2010.01191.x

Lessard, J., and G. Sauvageau. 2003. Bmi-1 determines the proliferative capacity of normal and leukaemic stem cells. *Nature.* 423:255–260. http://dx.doi.org/10.1038/nature01572

Lessard, J., A. Schumacher, U. Thorsteinsdottir, M. van Lohuizen, T. Magnuson, and G. Sauvageau. 1999. Functional antagonism of the Polycomb-Group genes eed and Bmi1 in hemopoietic cell proliferation. *Genes Dev.* 13:2691–2703. http://dx.doi.org/10.1101/gad.13.20.2691

Levine, R.L., and D.G. Gilliland. 2008. Myeloproliferative disorders. *Blood.* 112:2190–2198. http://dx.doi.org/10.1182/blood-2008-03-077966

Majewski, I.J., M.E. Blewitt, C.A. de Graaf, E.J. McManus, M. Bahlo, A.A. Hilton, C.D. Hyland, G.K. Smyth, J.E. Corbin, D. Metcalf, et al. 2008. Polycomb repressive complex 2 (PRC2) restricts hematopoietic stem cell activity. *PLoS Biol.* 6:e93. http://dx.doi.org/10.1371/journal.pbio.0060093

Martinez, A.M., B. Schuettengruber, S. Sakr, A. Janic, C. Gonzalez, and G. Cavalli. 2009. Polyhomeotic has a tumor suppressor activity mediated by repression of Notch signaling. *Nat. Genet.* 41:1076–1082. http://dx.doi.org/10.1038/ng.414

Martyré, M.C., N. Romquin, M.C. Le Bousse-Kerdiles, S. Chevillard, B. Benyahia, B. Dupriez, J.L. Demory, and F. Bauters. 1994. Transforming growth factor-beta and megakaryocytes in the pathogenesis of idiopathic myelofibrosis. *Br. J. Haematol.* 88:9–16. http://dx.doi.org/10.1111/j.1365-2141.1994.tb04970.x

Mochizuki-Kashio, M., Y. Mishima, S. Miyagi, M. Negishi, A. Saraya, T. Konuma, J. Shinga, H. Koseki, and A. Iwama. 2011. Dependency on the polycomb protein Ezh2 distinguishes fetal from adult hematopoietic stem cells. *Blood* Oct 31. [Epub ahead of print]. http://dx.doi.org/10.1182/blood-2011-03-340554

Molofsky, A.V., R. Pardal, T. Iwashita, I.K. Park, M.F. Clarke, and S.J. Morrison. 2003. Bmi-1 dependence distinguishes neural stem cell self-renewal from progenitor proliferation. *Nature.* 425:962–967. http://dx.doi.org/10.1038/nature02060

Morin, R.D., N.A. Johnson, T.M. Severson, A.J. Mungall, J. An, R. Goya, J.E. Paul, M. Boyle, B.W. Woolcock, F. Kuchenbauer, et al. 2010. Somatic mutations altering EZH2 (Tyr641) in follicular and diffuse large B-cell lymphomas of germinal-center origin. *Nat. Genet.* 42:181–185. http://dx.doi.org/10.1038/ng.518

Nikoloski, G., S.M. Langemeijer, R.P. Kuiper, R. Knops, M. Massop, E.R. Tönnissen, A. van der Heijden, T.N. Scheele, P. Vandenberghe, T. de Witte, et al. 2010. Somatic mutations of the histone methyltransferase gene EZH2 in myelodysplastic syndromes. *Nat. Genet.* 42:665–667. http://dx.doi.org/10.1038/ng.620

Published February 20, 2012

Oguro, H., A. Iwama, Y. Morita, T. Kamijo, M. van Lohuizen, and H. Nakauchi. 2006. Differential impact of *Ink4a* and *Arf* on hematopoietic stem cells and their bone marrow microenvironment in Bmi1-deficient mice. *J. Exp. Med.* 203:2247–2253. http://dx.doi.org/10.1084/jem.20052477

Oguro, H., J. Yuan, H. Ichikawa, T. Ikawa, S. Yamazaki, H. Kawamoto, H. Nakauchi, and A. Iwama. 2010. Poised lineage specification in multipotential hematopoietic stem and progenitor cells by the polycomb protein Bmi1. *Cell Stem Cell.* 6:279–286. http://dx.doi.org/10.1016/j.stem.2010.01.005

Park, I.K., D. Qian, M. Kiel, M.W. Becker, M. Pihalja, I.L. Weissman, S.J. Morrison, and M.F. Clarke. 2003. Bmi-1 is required for maintenance of adult self-renewing haematopoietic stem cells. *Nature.* 423:302–305. http://dx.doi.org/10.1038/nature01587

Pietersen, A.M., and M. van Lohuizen. 2008. Stem cell regulation by polycomb repressors: postponing commitment. *Curr. Opin. Cell Biol.* 20:201–207. http://dx.doi.org/10.1016/j.ceb.2008.01.004

Sauvageau, M., and G. Sauvageau. 2010. Polycomb group proteins: multi-faceted regulators of somatic stem cells and cancer. *Cell Stem Cell.* 7:299–313. http://dx.doi.org/10.1016/j.stem.2010.08.002

Serrano, M., H. Lee, L. Chin, C. Cordon-Cardo, D. Beach, and R.A. DePinho. 1996. Role of the INK4a locus in tumor suppression and cell mortality. *Cell.* 85:27–37. http://dx.doi.org/10.1016/S0092-8674(00)81079-X

Simon, J.A., and R.E. Kingston. 2009. Mechanisms of polycomb gene silencing: knowns and unknowns. *Nat. Rev. Mol. Cell Biol.* 10:697–708 http://dx.doi.org/10.1038/nrm2763.

Tefferi, A., J. Thiele, A. Orazi, H.M. Kvasnicka, T. Barbui, C.A. Hanson, G. Barosi, S. Verstovsek, G. Birgegard, R. Mesa, et al. 2007. Proposals and rationale for revision of the World Health Organization diagnostic criteria for polycythemia vera, essential thrombocythemia, and primary myelofibrosis: recommendations from an ad hoc international expert panel. *Blood.* 110:1092–1097. http://dx.doi.org/10.1182/blood-2007-04-083501

van der Lugt, N.M., J. Domen, K. Linders, M. van Roon, E. Robanus-Maandag, H. te Riele, M. van der Valk, J. Deschamps, M. Sofroniew, M. van Lohuizen, and A. Berns. 1994. Posterior transformation, neurological abnormalities, and severe hematopoietic defects in mice with a targeted deletion of the bmi-1 proto-oncogene. *Genes Dev.* 8:757–769. http://dx.doi.org/10.1101/gad.8.7.757

Young, A.R., and M. Narita. 2007. Oncogenic HMGA2: short or small? *Genes Dev.* 21:1005–1009. http://dx.doi.org/10.1101/gad.1554707

Yuan, J., M. Takeuchi, M. Negishi, H. Oguro, H. Ichikawa, and A. Iwama. 2011. Bmi1 is essential for leukemic reprogramming of myeloid progenitor cells. *Leukemia.* 25:1335–1343. http://dx.doi.org/10.1038/leu.2011.85

Published OnlineFirst on January 31, 2012; DOI:10.1158/0008-5472.CAN-11-3024

Cancer Research

Modulation of Glucose Metabolism by CD44 Contributes to Antioxidant Status and Drug Resistance in Cancer Cells

Mayumi Tamada, Osamu Nagano, Seiji Tateyama, et al.

Cancer Res Published OnlineFirst January 31, 2012.

Published OnlineFirst on January 31, 2012; DOI:10.1158/0008-5472.CAN-11-3024

Molecular and Cellular Pathobiology

Cancer Research

Modulation of Glucose Metabolism by CD44 Contributes to Antioxidant Status and Drug Resistance in Cancer Cells

Mayumi Tamada[1,2], Osamu Nagano[1,3], Seiji Tateyama[6], Mitsuyo Ohmura[2], Toshifumi Yae[1,3,5], Takatsugu Ishimoto[1,3,7], Eiji Sugihara[1,3], Nobuyuki Onishi[1], Takehiro Yamamoto[2], Hiroshi Yanagawa[6], Makoto Suematsu[2,4], and Hideyuki Saya[1,3]

Abstract

An increased glycolytic flux accompanied by activation of the pentose phosphate pathway (PPP) is implicated in chemoresistance of cancer cells. In this study, we found that CD44, a cell surface marker for cancer stem cells, interacts with pyruvate kinase M2 (PKM2) and thereby enhances the glycolytic phenotype of cancer cells that are either deficient in p53 or exposed to hypoxia. CD44 ablation by RNA interference increased metabolic flux to mitochondrial respiration and concomitantly inhibited entry into glycolysis and the PPP. Such metabolic changes induced by CD44 ablation resulted in marked depletion of cellular reduced glutathione (GSH) and increased the intracellular level of reactive oxygen species in glycolytic cancer cells. Furthermore, CD44 ablation enhanced the effect of chemotherapeutic drugs in p53-deficient or hypoxic cancer cells. Taken together, our findings suggest that metabolic modulation by CD44 is a potential therapeutic target for glycolytic cancer cells that manifest drug resistance. *Cancer Res; 72(6); 1–11. ©2012 AACR.*

Introduction

Most cancer cells depend primarily on glycolysis for their energy production regardless of the availability of oxygen. This unique metabolism is known as aerobic glycolysis called "Warburg effect" (1, 2). The glycolytic energetics under mitochondrial respiratory suppression in cancer cells reduces production of reactive oxygen species (ROS) and thereby confers resistance to various therapies. Indeed, interventions to tumors for switching from glycolysis to mitochondrial respiration were found to reduce tumor mass (3), suggesting that aerobic glycolysis is an important feature of cancer cells distinct from normal cells. However, precise mechanisms underlying the switch to use of glycolysis for energy production in cancer cells remain unclear.

Dysfunction of p53, which frequently occurs in human cancers, promotes aerobic glycolysis, because p53 positively regulates mitochondrial respiration through inducing cytochrome *c* oxidase 2 expression (4). Furthermore, p53 dysfunction has recently been shown to increase metabolic flux to pentose phosphate pathway (PPP; ref. 5).

CD44 is a major adhesion molecule and has been implicated in various biologic processes including cell migration and cell proliferation, as well as tumor growth and metastasis (6–8). CD44 is a cell surface marker for cancer stem cells, and CD44-expressing cancer cells are able to initiate tumors in some types of cancer (9). We recently showed that splice variant forms of CD44 (CD44v) inhibit ROS accumulation in cancer cells, thereby promoting tumor growth (10). Recent findings suggest that p53 not only regulates glucose metabolism but induces CD44 expression (6). The fact raises a possibility that CD44 is involved in regulating glycolytic pathway, whereas the functional relevance of CD44 to the characteristic aerobic glycolysis of cancer cells remains unknown.

With the use of *in vitro* virus (IVV) selection screening, we have shown that CD44 interacts with PKM2, which has been recently implicated in Warburg effect (11–14). Expression of CD44 enhanced the glycolytic phenotype of p53-deficient or hypoxic cancer cells and promoted metabolic flux to PPP and thereby increased glutathione (GSH) levels. We thus propose that CD44 plays a role in metabolic shift via regulation of PKM2 and ROS protection in cancer cells.

Materials and Methods

Cell lines

Human colorectal cancer cell HCT116 harboring wild-type p53 (p53WT) and its isogenic derivative lacking p53 (p53KO) were kindly provided by Dr. B. Vogelstein (Johns Hopkins Oncology Center, Baltimore, MD). Human glioma cell U251MG and human lung carcinoma cell A549 were obtained from American Type Culture Collection. The cell lines used were

Authors' Affiliations: [1]Division of Gene Regulation, Institute for Advanced Medical Research, [2]Department of Biochemistry, School of Medicine, Keio University; [3]Japan Science and Technology Agency, Core Research for Evolutional Science and Technology (CREST); [4]Japan Science and Technology Agency, ERATO, Suematsu Gas Biology Project; [5]Department of Respiratory Medicine, Juntendo University, Tokyo, Japan; [6]Department of Biosciences and Informatics, Faculty of Science and Technology, Keio University, Kanagawa, Japan; and [7]Department of Gastroenterological Surgery, Graduate School of Medical Sciences, Kumamoto University, Kumamoto, Japan

Note: Supplementary data for this article are available at Cancer Research Online (http://cancerres.aacrjournals.org/).

Corresponding Author: Hideyuki Saya, Division of Gene Regulation, Institute for Advanced Medical Research, School of Medicine, Keio University, 35 Shinano-machi, Shinjuku-ku, Tokyo 160-8582, Japan. Phone: 81-3-5363-3981; Fax: 81-3-5363-3982; E-mail: hsaya@a5.keio.jp

doi: 10.1158/0008-5472.CAN-11-3024

Published OnlineFirst on January 31, 2012; DOI:10.1158/0008-5472.CAN-11-3024

tested and authenticated on the basis of an STR Multiplex method that uses 9 different loci: D5S818, D13S317, D7S820, D16S539, vWA, THOI, Amelogenin, TPOX, and CSFIPO (PowerPlex 1.2 system, Promega Corporation). Cells were stored and used within 3 months after resuscitation of frozen aliquots.

RNA interference

Depletion of CD44 and xCT siRNA was conducted as previously described (10).

Measurement of cell doubling time

Cells were cultured under 5% CO_2 at 37°C. The number of viable cells was determined every 24 hours by staining with trypan blue. Doubling time was calculated by using the equation shown in Supplementary Materials and Methods. Data are means ± SD from 3 independent experiments.

Cell proliferation assay

Cell proliferation was measured at 24 and 72 hours with the use of an XTT cell proliferation assay kit (Biological Industries). Data are means ± SD from 6 independent experiments.

Measurement of ATP production, glucose consumption, lactate production

Cellular ATP level was determined with the use of luminescence-based assay (ATPlite; Perkin Elmer). ATP generation was normalized by the cell number. Glucose and lactate concentrations of the cultured medium were measured by using glucose oxidase–based assay kit (Sigma) and F-kit L-Lactate (J.K. International), respectively. Glucose consumption and lactate production were corrected by amounts of cellular protein. Data are means ± SD from 6 independent experiments.

IVV screening and GST pull-down assay

IVV selection and glutathione *S*-transferase (GST) pull-down assay were conducted as described previously (15–17). The cDNA library for screening was obtained from U251MG cells. The intracellular domain of CD44 (CD44ICD) was prepared as a bait protein. Details are shown in Supplementary Materials and Methods.

Immunoprecipitation and immunoblot analysis

Immunoprecipitation was conducted with the use of anti-CD44 antibodies (F10-44-2 and IM7) or rabbit monoclonal antibody to PKM2, and the resulting precipitates were subjected to immunoblot analysis as previously described (10). The intensity of the band was measured using by Multi Gauge software Ver.3.1 (FujiFilm). Data are means ± SD from 3 independent experiments.

Pyruvate kinase activity assay

Pyruvate kinase activity was determined by using a pyruvate oxidase-based assay kit (BioVision). Data are means ± SD from 5 independent experiments.

Measurement of glucose metabolites

Intracellular metabolites of glucose were measured by capillary electrophoresis combined with mass spectrometry (CE/MS; Agilent Technology) as previously described (18, 19). To measure fluxes of glucose metabolites, the cells were incubated for 10 or 30 minutes in the presence of D-($^{13}C_6$) glucose (4.5 g/L; ISOTEC) and then lysed for determination of the amounts of the labeled D-glucose incorporated into the cells. Data are means ± SD from 3 independent experiments. Details are shown in Supplementary Materials and Methods.

Measurement of mitochondrial membrane potential and mitochondrial superoxide production

Mitochondrial membrane potential ($\Delta\psi m$) and mitochondrial superoxide production were measured in live cells by using tetramethylrhodamine methyl ester perchlorate (TMRM) or MitoSOX Red indicator (Molecular Probes), respectively. Cells were incubated with 200 nmol/L TMRM or 5 μmol/L MitoSOX and subjected to quantification of the mean intensity of fluorescence in more than 500 cells by using a Biorevo BZ-9000 fluorescence microscope (Keyence) and analysis software. Nuclei were stained with Hoechst 33342 for fluorescence microscopy. Data are means ± SD from a representative experiment.

Measurement of glucose uptake (2-NBDG uptake)

Cells were subjected to staining with 2-(*N*-(7-nitrobenz-2-oxa-1,3-diazol-4-yl)amino)-2-deoxyglucose (2-NBDG; Molecular Probes) as described previously (20). 2-NBDG fluorescence intensity was determined for more than 500 cells in each experiment. Data are means ± SD from a representative experiment.

Quantitative and semiquantitative real-time reverse transcriptase (RT)-PCR analysis

Quantitative PCR analysis was conducted as previously described (10). Data were normalized by the amount of *HPRT1* mRNA. Data are means ± SD of 3 independent experiments. Primer sequences are described in Supplementary Materials and Methods.

Immunofluorescence analysis

Immunofluorescence analysis of cultured cells was conducted as previously described (10).

Measurement of GSH and ROS

Intracellular levels of GSH and ROS were determined by using GSH-Glo Glutathione Assay Kit (Promega) and 2′,7′-dichlorofluorescein-diacetate (DCF-DA), respectively, as described previously (10).

Drug treatment and cell death analysis

Cells were exposed to anticancer drugs for 48 hours at 37°C under 21% O_2 and 5% CO_2 (normoxia) or under 1% O_2 and 5% CO_2 (hypoxia). Sub-G_1 assessment based on cell-cycle analysis was conducted as described previously (21). In addition, cell death was evaluated by the trypan blue dye exclusion (22).

Statistical analysis

Data are presented as means ± SD and were analyzed with the unpaired Student *t* test by using Excel 2007 (Microsoft). A P value of <0.05 was considered statistically significant.

Published OnlineFirst on January 31, 2012; DOI:10.1158/0008-5472.CAN-11-3024

Results

CD44 regulates cell proliferation and energy production in glycolytic cancer cells

To understand roles of CD44 in cancer cell proliferation, we examined effects of CD44 ablation by RNA interference on proliferation in 2 human cancer cells having wild-type p53 (HCT116 p53WT and A549) and 2 p53-deficient cancer cells (HCT116 p53KO and U251MG; Supplementary Fig. S1A and S1B). CD44 depletion caused inhibition of proliferation of p53-deficient cells, whereas it did not affect that of p53WT cells (Fig. 1A; Supplementary Fig. S1C and S1D). Trypan blue staining confirmed that decreases in growth rates of p53-deficient cells resulting from CD44 ablation were not attributable to the induction of apoptosis (data not shown). These results suggest that CD44 contributes to proliferation of p53-deficient cancer cells.

Given that energy production is necessary for proliferation, we examined whether CD44 expression affects ATP levels. CD44 ablation decreased in ATP contents of p53-deficient cells but not in those of p53WT cells (Fig. 1B), suggesting that CD44 regulates energy production in p53-deficient cells. The source of ATP production in cancer cells has been found to differ depending on p53 status (4). Consistent with previous observations (4, 5), we found that HCT116 p53KO cells manifest a glycolytic phenotype, characterized by increased glucose consumption, lactate production, and expression of the glucose transporter Glut1 (Supplementary Fig. S1E and S1G). CD44 ablation resulted in a decrease in glucose consumption

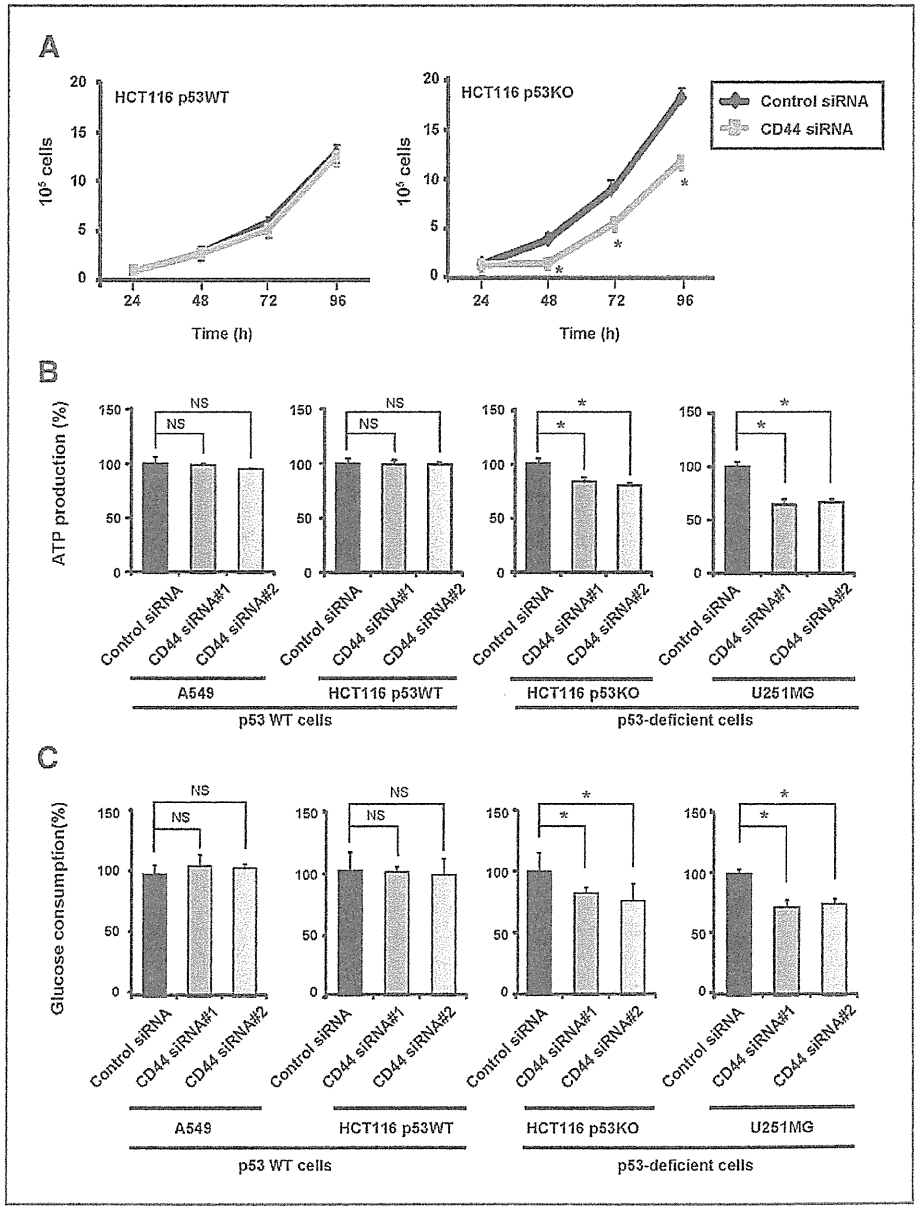

Figure 1. CD44 ablation suppresses cell proliferation and decreases ATP production in p53-deficient cancer cells. A, time course analysis of cell growth beginning after transfection with control and CD44 siRNAs for 48 hours. *, $P < 0.005$. B and C, ATP production and glucose consumption in cells cultured for 24 hours after transfection with indicated siRNAs for 48 hours. Data are expressed as a percentage of the value for control siRNA cells. *, $P < 0.001$. NS, not significant.

Published OnlineFirst on January 31, 2012; DOI:10.1158/0008-5472.CAN-11-3024

in p53-deficient cells but not in p53WT cells (Fig. 1C). We therefore hypothesized that CD44 increases energy production in p53-deficient cells by promoting glycolysis.

CD44 interacts with PKM2 and inhibits its activity to maintain the glycolytic phenotype in cancer cells

To investigate mechanisms by which CD44 regulates glycolysis, we attempted to identify CD44-interacting molecules that participate in glycolysis by IVV screening (Supplementary Fig. S2A). The cDNA library for screening was obtained from U251MG cells, which manifests the glycolytic phenotype because of p53 mutation. The intracellular domain of CD44 (CD44ICD) was prepared as a bait protein. Among 292 candidate CD44ICD-binding proteins identified by the IVV screening, we focused on PKM2, a molecule regulating aerobic glycolysis and tumor growth (11). Sequencing revealed that 2 selected PKM2 clones, designated 61–17C, encoded the 61 NH_2-terminal amino acids of PKM2 fused with 18 amino acids translated from the 5′-untranslated region of the *PKM2* gene (Supplementary Fig. S2B). To determine whether CD44ICD interacts with the NH_2-terminal region or with the protein fragment encoded by the 5′-untranslated region, we prepared 4 GST fusion proteins containing full-length, the 61–17C fragment, the 61 NH_2-terminal residues (N61AA), and a deletion mutant lacking residues 1 to 61 (ΔN61AA; Supplementary Fig. S2C) and subjected these fusion proteins to a pull-down assay with recombinant CD44ICD. The assay revealed that CD44ICD bound to full-length PKM2, to 61–17C, and to N61AA, but not to ΔN61AA (Fig. 2A),

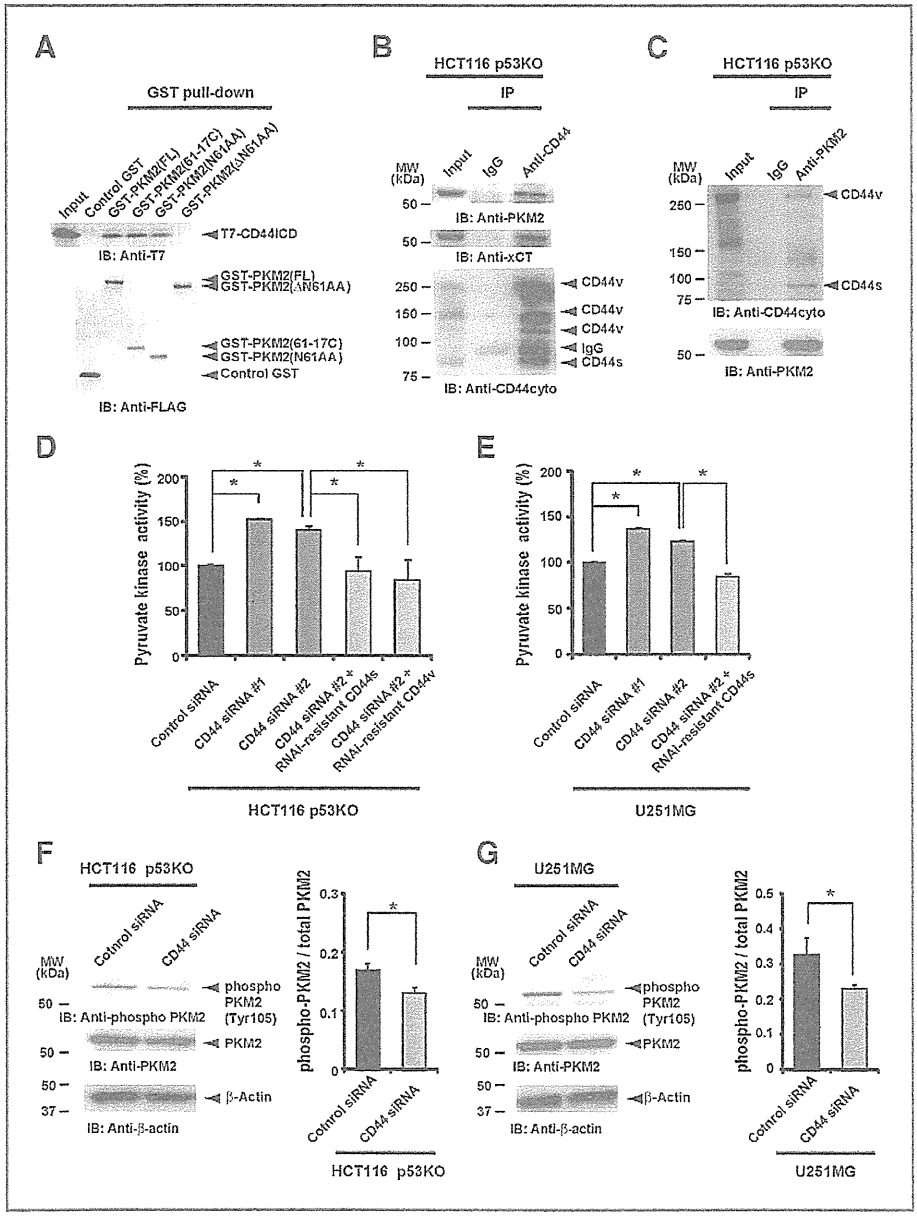

Figure 2. CD44 contributes to the glycolytic phenotype of cancer cells through interaction with PKM2. A, the GST–PKM2 fusion proteins were subjected to a pull-down assay with T7-tagged CD44ICD. The bead-bound proteins as well as the T7-CD44ICD input to the binding mixtures (Input) were subjected to immunoblot (IB) analysis with indicated antibodies. FL, full-length. B and C, the cell lysates were subjected to immunoprecipitation (IP) with indicated antibody and the resulting precipitates as well as the original cell lysates (Input) were immunoblotted with indicated antibodies. D and E, enzymatic activity of pyruvate kinase in cells transfected for 72 hours with indicated siRNAs or with both a CD44 siRNA#2 and an expression vector for a corresponding RNA interference (RNAi)–resistant form of CD44s or CD44v. *, $P < 0.001$. F and G, lysates of cells transfected with indicated siRNAs for 48 hours were immunoblotted with indicated antibodies. The graphs indicate the ratio of phosphorylation to total PKM2.*, $P < 0.05$. MW, molecular weight.

Published OnlineFirst on January 31, 2012; DOI:10.1158/0008-5472.CAN-11-3024

indicating that CD44ICD interacts directly to the NH_2-terminal region of PKM2 encompassing residues 1 to 61. We also conducted immunoprecipitation analysis to verify the interaction between endogenous CD44 and PKM2 proteins. PKM2 was coimmunoprecipitated with CD44 (Fig. 2B), as was the cystine transporter xCT, which was previously shown to interact with CD44 (10), and confirmed that both CD44v and CD44s were coimmunoprecipitated with PKM2 (Fig. 2C).

Given that low activity of PKM2 is thought to promote aerobic glycolysis (11, 12), we examined that whether CD44 expression affects PKM2 activity. CD44 ablation in glycolytic cancer cells increased the PKM2 activity (Fig. 2D and E). In addition, the expression of siRNA-resistant form of CD44s or CD44v in CD44-depleted cells (Supplementary Fig. S2D) significantly inhibited the increase in PKM2 activity induced by ablation of endogenous CD44 (Fig. 2D and E). Tyrosine phosphorylation (Tyr105) of PKM2 was reported to suppress PKM2 activity (12, 13). We found that CD44 ablation reduced Tyr105 phosphorylation of PKM2 (Fig. 2F and G). These data suggested that the CD44/PKM2 interaction suppresses PKM2 activity through increasing its phosphorylation and thereby promotes the glycolytic phenotype in p53-deficient cancer cells.

CD44 ablation induces a metabolic shift to mitochondrial respiration in glycolytic cancer cells

To examine effects of CD44 expression on glucose metabolism, we conducted metabolomic analysis by loading the cells with D-($^{13}C_6$)glucose. CD44 ablation increased amounts of metabolites in tricarboxylic acid (TCA) cycle (Fig. 3A), suggesting that CD44 expression limits metabolic flux to the cycle. Furthermore, we measured the production of lactate, the final product of glycolysis, and found that CD44 ablation reduced lactate production in p53KO cells (Fig. 3B), Collectively, our results suggested that CD44 ablation induces a metabolic shift from aerobic glycolysis to mitochondrial respiration in cancer cells.

It has been reported that the suppression of mitochondrial respiration is characterized by high intensity staining of $\Delta\psi$m-sensitive dye TMRM and low mitochondrial ROS (3). To confirm the CD44-mediated metabolic shift, we conducted cell staining with TMRM and a fluorescent probe for mitochondrial superoxide (MitoSOX). CD44 ablation significantly reduced the intensity of TMRM staining and increased the mitochondrial ROS levels (Fig. 3C and D). Effects similar to those of CD44 ablation were obtained by treatment with dichloroacetate (DCA; Supplementary Fig. S3A and S3B), which inhibits mitochondrial pyruvate

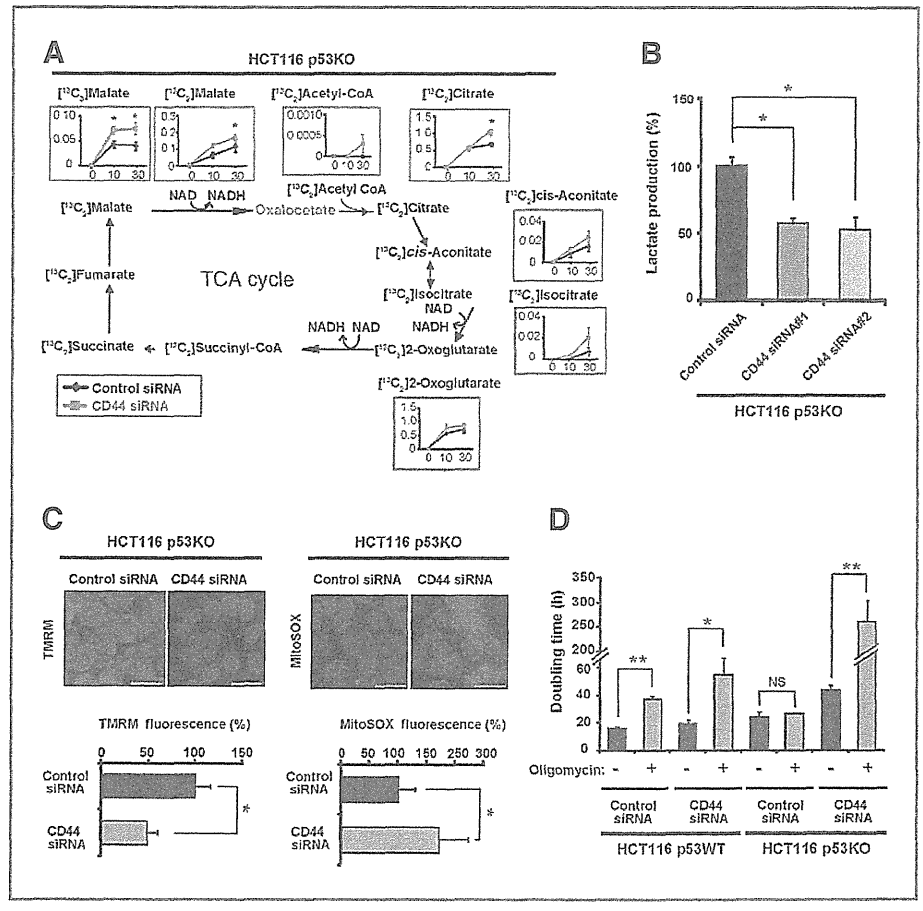

Figure 3. CD44 ablation induces a metabolic shift from glycolysis to mitochondrial respiration in glycolytic cancer cells. A, metabolomic analysis of cells incubated for 24 hours after transfection with indicated siRNAs for 48 hours and then labeled with D-($^{13}C_6$) glucose. The amounts of the indicated metabolites of the TCA cycle were measured. *, $P < 0.05$. B, lactate production by cells cultured for 24 hours after transfection with siRNAs for 48 hours. *, $P < 0.001$. C and D, $\Delta\psi$m and mitochondrial ROS production in cells that had been transfected with siRNAs for 48 hours. Scale bars, 20 μm. *, $P < 0.001$. E, doubling time of the cells that had been transfected with siRNAs for 48 hours was determined during subsequent incubation of the cells in the absence or presence of 125 nmol/L oligomycin. *, $P < 0.01$; **, $P < 0.001$. NS, not significant.

Published OnlineFirst on January 31, 2012; DOI:10.1158/0008-5472.CAN-11-3024

dehydrogenase kinase and thereby shifts glucose metabolism from glycolysis to mitochondrial respiration (3). These data therefore suggested that, like DCA treatment, CD44 ablation promotes mitochondrial respiration in glycolytic cancer cells.

To analyze further the metabolic shift in CD44-depleted cancer cells, we investigated the sensitivity of the cells to oligomycin, an inhibitor of mitochondrial ATP synthesis. Oligomycin inhibited the proliferation of p53WT cells, which depend more on mitochondrial respiration, whereas it did not affect the proliferation of p53KO cells (Fig. 3E). However, p53KO cells became sensitive to oligomycin by CD44 ablation (Fig. 3E), suggesting that loss of CD44 suppresses their glycolytic phenotype and renders them more dependent on mitochondrial respiration.

CD44 ablation reduces glucose uptake and PPP flux

In addition to the metabolic shift, we found that CD44 ablation reduced metabolic flux to the PPP. In particular, CD44 depletion resulted in a reduced amount of the PPP metabolite 6-phosphogluconate (6-PG) in p53KO cells (Fig. 4A). However, the expression of glucose-6-phosphate dehydrogenase (G6PD), a key enzyme that catalyzes the first step of PPP, was not affected by CD44 depletion (Supplementary Fig. S4A). The data showing that CD44 ablation reduced combined amounts of G6P and fructose 6-phosphate (F6P; Supplementary Fig. S4B) led us to speculate that reduced PPP fluxes in CD44-deficient cells result from lack of glucose. Indeed, we found that CD44 ablation led to suppression of glucose uptake (Fig. 4B), which may contribute to reduced PPP fluxes in CD44-depleted cells.

Given that glucose uptake is mainly mediated by Glut1 in cancer cells (23, 24), we examined Glut1 expression in CD44-depleted cells. Indeed, CD44 depletion resulted in downregulation of Glut1 expression (Fig. 4C and D). Pharmacologic inhibition of mitochondrial respiration was previously shown to increase glucose uptake potentially through upregulation of Glut1 expression (25, 26). We therefore hypothesized that CD44 ablation suppresses Glut1 expression as a result of the induced metabolic shift from glycolysis to mitochondrial respiration. Consistent with this hypothesis, the downregulation of Glut1 expression induced by CD44 ablation was reversed by treatment with rotenone, an inhibitor of complex I of the mitochondrial respiratory chain (Fig. 4C and D). The enhancement of mitochondrial respiration induced by CD44 ablation may suppress Glut1 expression, thereby reducing glucose uptake and PPP fluxes in cancer cells (Supplementary Fig. S4C).

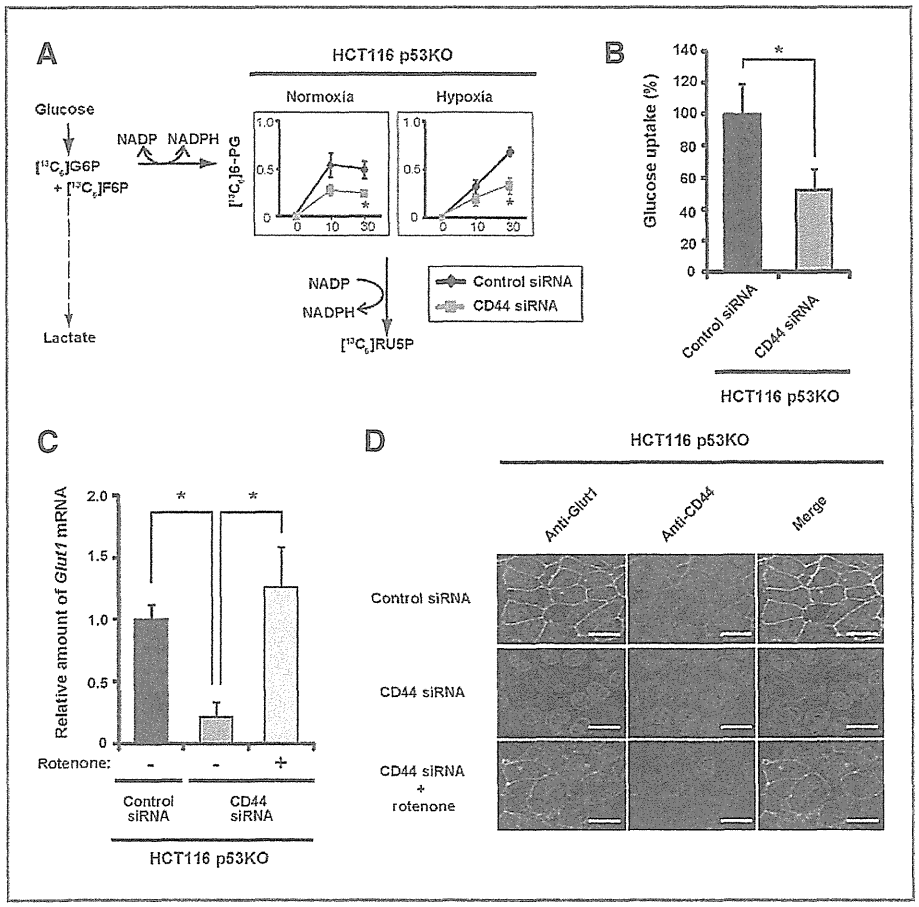

Figure 4. CD44 ablation suppresses glucose uptake leading to reduced flux to PPP. A, metabolomic analysis of cells incubated for 24 hours under normoxia or hypoxia after transfection with indicated siRNA for 48 hours. *, $P < 0.05$. Parts of the glycolytic pathway and PPP are indicated on the left and right, respectively. RU5P, ribulose-5-phosphate. B, glucose uptake in cells transfected with siRNAs. *, $P < 0.001$. C, quantitative RT-PCR analysis of *Glut1* mRNA in cells transfected with siRNAs for 48 hours and then incubated in the absence or presence of 5 μmol/L rotenone for 2 hours. *, $P < 0.001$. D, immunofluorescence analysis of Glut1 and CD44 expression in cells transfected with siRNAs for 48 hours and then incubated in the absence or presence of 5 μmol/L rotenone for 12 hours. Scale bars, 20 μm.

Published OnlineFirst on January 31, 2012; DOI:10.1158/0008-5472.CAN-11-3024

Reduced PPP flux by CD44 ablation depletes GSH and increases ROS

Considering that the PPP generates NADPH which is essential for generating GSH, we measured GSH levels in CD44-depleted cells. CD44 ablation significantly reduced GSH contents of p53KO cells (Fig. 5A). We have recently found that CD44v promotes xCT-mediated cystine uptake and thereby increases GSH synthesis (10). The depletion of GSH apparent in CD44-deficient HCT116 p53KO cells, which express both CD44s and CD44v, might therefore have been attributable to

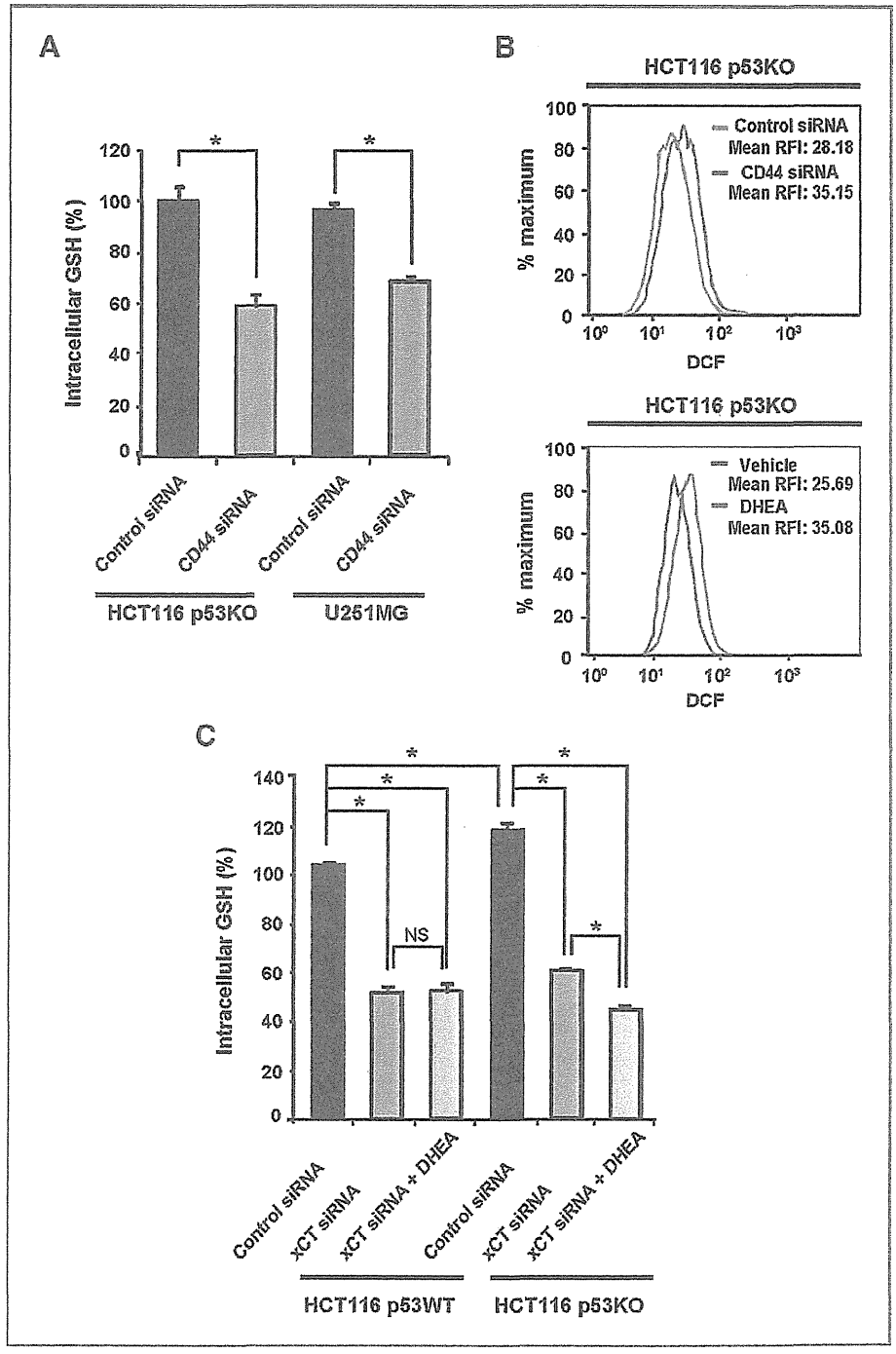

Figure 5. CD44 ablation reduces GSH level through suppression of not only cystine uptake but also flux to PPP, leading to ROS production in glycolytic cancer cells. A, intracellular GSH level in cells cultured for 12 hours after transfection with indicated siRNAs for 48 hours. *, $P < 0.001$. B, cellular ROS level was measured with the use of DCFH-DA and flow cytometry in cells that had either been transfected with siRNAs for 72 hours or been incubated in the presence of 30 μmol/L DHEA or vehicle for 24 hours. The mean relative fluorescence intensity (RFI) values are shown. C, intracellular GSH level in cells cultured for 12 hours in absence or presence of 30 μmol/L DHEA after transfection with siRNAs for 48 hours and pretreatment of the cells with DHEA for 24 hours. *, $P < 0.001$. DCF, dichlorofluorescin, the fluorescent product produced by ROS; NS, not significant.

Published OnlineFirst on January 31, 2012; DOI:10.1158/0008-5472.CAN-11-3024

downregulation of cystine uptake. To rule out this possibility, we measured GSH levels in CD44-depleted U251MG cells, which express CD44s but not CD44v (ref. 27; Supplementary Fig. S1B). CD44 ablation in U251MG cells also resulted in a significant decrease in GSH levels (Fig. 5A). These findings suggested that CD44 increases cellular GSH contents not only through promotion of xCT-mediated cystine uptake but also by maintenance of the PPP flux and consequent NADPH production in cancer cells.

GSH is a major metabolite protecting against oxidative stress. We found that intracellular ROS levels were increased in CD44-depleted p53KO cells comparable with those in p53KO cells treated with dehydroepiandrosterone (DHEA), a PPP inhibitor (Fig. 5B). In contrast, although CD44 ablation decreased in GSH levels (Supplementary Fig. S5A), it did not affect intracellular ROS accumulation in p53WT cells (Supplementary Fig. S5B). Given that CD44 ablation inhibits neither uptake (data not shown) nor consumption of glucose (Fig. 1D) in p53WT cells, CD44 depletion might have a less pronounced effect on flux to the PPP in p53WT cells than it does in p53KO cells. This hypothesis is supported by the fact that DHEA treatment significantly conferred an additional reduction in GSH levels in the xCT-depleted p53KO cells whereas it did not provide the additional change in xCT-depleted p53WT cells (Fig. 5C). Together, these results suggested that CD44 limits ROS accumulation in glycolytic cancer cells, such as those with dysfunctional p53, by promoting cystine uptake and metabolic flux to PPP, leading to increase consequent GSH synthesis.

CD44 ablation sensitizes glycolytic cancer cells to anticancer drugs

Given that aerobic glycolysis and low ROS levels are associated with drug resistance in cancer cells (28), we examined whether CD44 ablation enhances the sensitivity of cancer cells to chemotherapeutic agents. Consistent with previous observations (29), cisplatin (CDDP) induced apoptotic cell death to a much greater extent in p53WT cells (sub-G_1 population, 56.71%) than in p53KO cells (sub-G_1 population, 15.28%; Fig. 6A). CD44 ablation was associated with enhancement of CDDP-induced cell death in p53KO cells but not in p53WT cells (Fig. 6A, Supplementary Fig. S6A). This increased sensitivity to CDDP conferred by CD44 ablation in p53KO cells was inhibited by pretreatment with *N*-acetylcysteine (NAC; Fig. 6A; Supplementary Fig. S6A), a precursor of GSH that functions as an antioxidant. In addition to CDDP, we obtained the similar data using adriamycin (ADM) and 5-fluorouracil (5-FU; Supplementary Fig. S6A). Furthermore, similar to the effect of CD44 ablation, the PPP inhibitor DHEA, which suppresses NADPH production and thereby increases ROS levels, also enhanced the sensitivity of p53KO cells to CDDP (Supplementary Fig. S6B). Together, these results indicated that CD44 ablation increased drug sensitivity, possibly by increasing ROS levels, in p53-deficient cells.

Given that, like p53 deficiency, hypoxia also promotes glycolysis and confers drug resistance in cancer cells (30, 31), we investigated whether CD44 ablation affects glucose metabolism and drug sensitivity under hypoxia. p53WT cells cultured under such conditions show more of a glycolytic phenotype, including increased Glut1 expression (Supplementary Fig. S6C), glucose consumption (Fig. 6B), and lactate production (Fig. 6C), compared with those cultured under normoxia. The sensitivity of these cells to anticancer drugs was also reduced on their exposure to hypoxia (Fig. 6A and D; Supplementary Fig. S6D). CD44 ablation reduced both glucose consumption and lactate production in hypoxic p53WT cells (Fig. 6B and C) as well as increased their sensitivity to anticancer drugs (Fig. 6D; Supplementary Fig. S6D), effects that were not observed under the normoxia (Figs. 1D, 6A and C; Supplementary Fig. S6A). These results thus indicated that CD44 plays an important role in resistance to chemotherapeutic drugs by maintaining the glycolytic phenotype and thereby suppressing ROS production in glycolytic cancer cells, such as those with p53 mutation or exposed to hypoxia. Metabolic modulation by CD44 ablation increases ROS production, thereby sensitizing highly glycolytic cancer cells to conventional chemotherapy.

Discussion

Our results indicate that the expression of CD44 affects proliferation through regulation of energy production in p53-deficient glycolytic cancer cells. In contrast, CD44 did not affect it in p53WT cancer cells, which obtain most of their energy through mitochondrial respiration. We therefore conclude that CD44 plays an important role in the regulation of glucose metabolism in cancer cells that show a glycolytic phenotype.

IVV screening is a powerful tool for identifying biologic macromolecules that participate in protein–protein interactions (15–17). By using this approach, we identified PKM2 as a mediator of the promotion of the glycolytic phenotype of cancer cells by CD44. CD44 ablation suppressed Tyr105 phophorylation of PKM2 and consequently increased the PKM2 activity. It is therefore possible that CD44 serves as a scaffold to facilitate the interaction between a tyrosine kinase and PKM2 near the cell membrane, thereby resulting in downregulation of PKM2 activity (Supplementary Fig. S7).

Consistent with the observation that CD44 ablation activated PKM2, the amounts of metabolites in the TCA cycle were increased in CD44-depleted cells. Furthermore, the increase of not only ($^{13}C_2$)malate but also ($^{13}C_3$)malate by CD44 ablation indicated the increment of TCA cycle flux. The findings support the idea that metabolic flux to TCA cycle is promoted by lacking CD44.

We found that CD44 ablation not only induced this metabolic shift but also reduced glucose uptake in cancer cells. It was previously reported that inhibition of mitochondrial respiration increases glucose uptake potentially through upregulation of Glut1 expression (25, 26), indicating that mitochondrial respiration is a regulatory factor for Glut1 expression. Therefore, we speculated that shift from glycolysis to mitochondrial respiration induced by CD44 ablation suppresses Glut1 expression (Supplementary Fig. S4C).

A reduction in glucose uptake has been shown to cause a decrease in flux to the PPP (32, 33). Accordingly, the

Published OnlineFirst on January 31, 2012; DOI:10.1158/0008-5472.CAN-11-3024

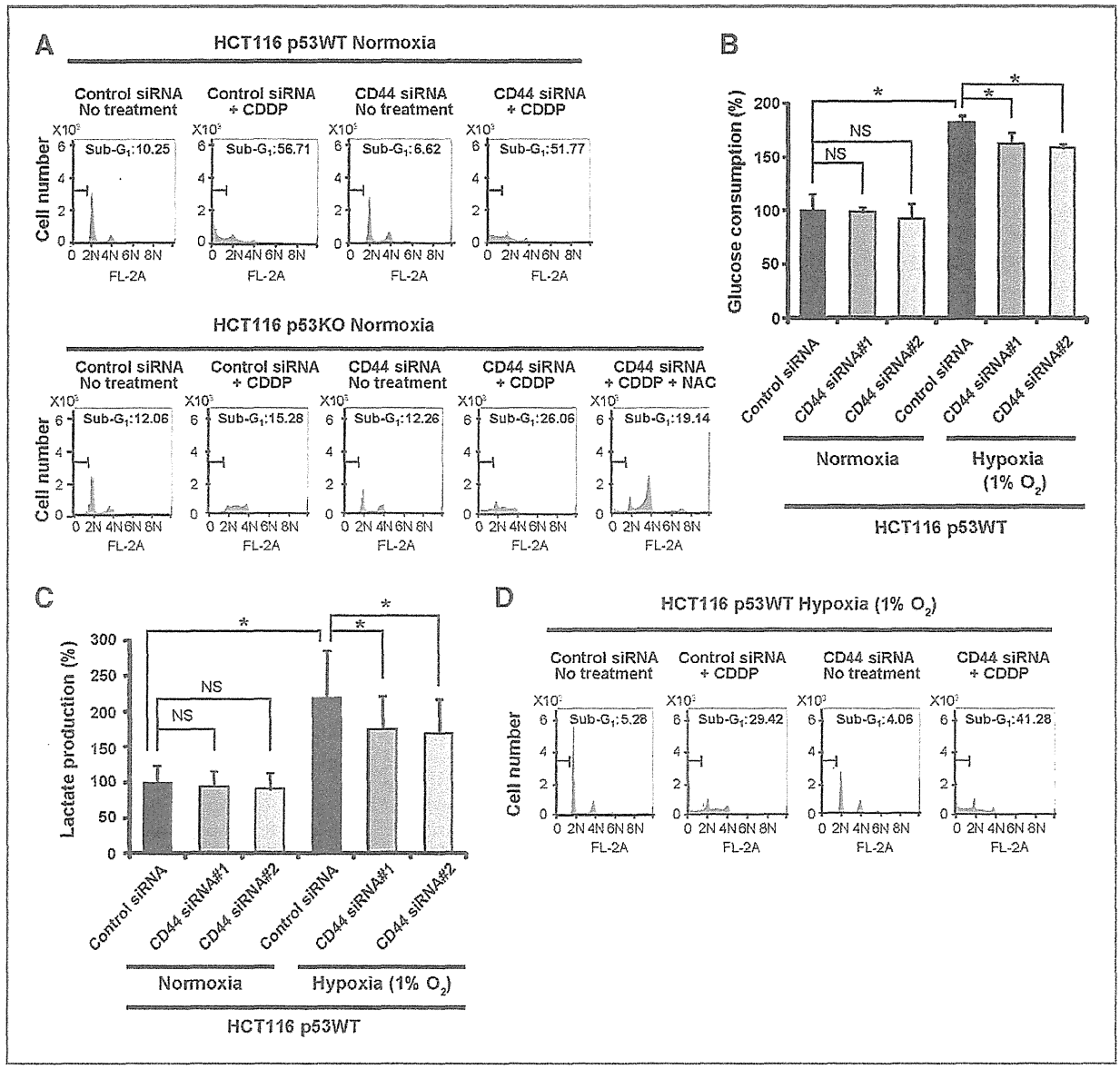

Figure 6. CD44 ablation increases sensitivity to CDDP in glycolytic cancer cells. A, flow cytometric analysis of cells that had been transfected with indicated siRNAs for 48 hours. The transfected cells were incubated for 48 hours in the absence or presence of 50 μmol/L CDDP under normoxia (21% O_2). The effect of CDDP was also assessed after pretreatment of the cells with 1 mmol/L NAC for 1 hour. The percentage of sub-G_1 cells was determined. B and C, glucose consumption and lactate production in cells cultured for 24 hours under normoxia and hypoxia after transfection with siRNAs for 48 hours. *, $P < 0.05$. D, flow cytometric analysis of cells that had been transfected with siRNAs for 48 hours under hypoxia. The transfected cells were incubated for 48 hours in the absence or presence of 50 μmol/L CDDP under hypoxia. NS, not significant.

downregulation of glucose uptake in CD44-depleted cells might lead to the reduced flux to the PPP. Because the PPP is a major source of NADPH which is required for regeneration of the antioxidant GSH (34), the metabolic regulation by CD44 in p53 dysfunctional cancer cells was found to affect GSH levels. We previously showed that CD44v expression promotes xCT-mediated cystine uptake and consequent GSH synthesis (10). In the present study, however, we found that CD44 ablation reduced the GSH levels in U251MG cells, which express only CD44s, as well as in HCT116 p53KO cells, which express both CD44s and CD44v. These results indicate that GSH synthesis is regulated not only by CD44v but also by CD44s. We suggest that CD44 maintains the GSH levels in glycolytic cancer cells through the combination of 2 mechanisms: enhancement of flux to the PPP by both CD44v and CD44s and promotion of xCT-mediated cystine uptake by CD44v (Supplementary Fig. S7).

In p53KO cells, CD44 ablation increased the intracellular ROS levels under the basal condition. However, in p53WT cells, which are less dependent on glycolysis, CD44 ablation

Published OnlineFirst on January 31, 2012; DOI:10.1158/0008-5472.CAN-11-3024

increased the ROS levels only when the cells were treated with H_2O_2 (10). Given that CD44 ablation did not reduce glucose uptake or glucose consumption in p53WT cells and that p53 inhibits the PPP (5), the depletion of GSH induced by CD44 ablation in p53WT cells might be mostly due to the suppression of cystine uptake via the xCT transporter.

CD44-expressing cancer cells including cancer stem cells show chemoresistance (35, 36). Anticancer drugs, such as CDDP, adriamycin, and 5-fluorouracil, are known to induce ROS generation and thereby trigger cell death (29, 37–39). Consistent with the results of previous studies (29, 31, 40–42), we found that the sensitivity of cancer cells to anticancer drugs is markedly affected by intrinsic and extrinsic factors such as p53 deficiency and hypoxia. These factors render cancer cells dependent on glycolysis. However, we further found that CD44 ablation enhanced effect of the anticancer drugs in p53KO cells and in hypoxic p53WT cells. We confirmed that the enhancement of drug sensitivity induced by CD44 ablation in p53KO cells was inhibited by NAC treatment. Furthermore, like CD44 ablation, treatment with DHEA also increased CDDP sensitivity. Therefore, CD44 ablation triggers a metabolic shift to mitochondrial respiration that is accompanied by suppression of both the PPP and xCT-mediated cystine uptake, leading to downregulation of GSH synthesis and a consequent increase in ROS production. Furthermore, these effects of CD44 ablation might function synergistically with chemotherapeutic drugs. The possibility that CD44-targeted therapy may perturb the metabolism of cancer stem–like cells and thereby impair their capacity to defend against ROS warrants further investigation.

Disclosure of Potential Conflicts of Interest

No potential conflicts of interest were disclosed.

Authors' Contributions

Conception and design: M. Tamada, O. Nagano, H. Saya
Development of methodology: M. Tamada, S. Tateyama, T. Yae
Acquisition of data (provided animals, acquired and managed patients, provided facilities, etc.): M. Tamada, S. Tateyama, M. Ohmura, T. Yae, T. Ishimoto, H, Yanagawa, M. Suematsu
Analysis and interpretation of data (e.g., statistical analysis, biostatistics, computational analysis): M. Tamada, M. Ohmura, T. Yae
Writing, review, and/or revision of the manuscript: M. Tamada, S. Tateyama, H. Yanagawa, M. Suematsu, H. Saya
Administrative, technical, or material support (i.e., reporting or organizing data, constructing databases): M. Tamada, T. Yae, E. Sugihara, N. Onishi, T. Yamamoto, H. Yanagawa, M. Suematsu
Study supervision: H. Saya

Acknowledgments

The authors thank K. Arai for help with preparation of the manuscript and K. Dan, M. Fujiwara, and K. Matsuo (Core Instrumentation Facility), S. Suzuki and Y. Matsuzaki (Department of Physiology), T. Matsu-ura, Y. Nagahata, T. Hishiki, A. Kubo, Y.A Minamishima, and M. Kajimura (Department of Biochemistry, School of Medicine, Keio University, Tokyo, Japan) for discussion and technical assistance.

Grant Support

This work was supported in part by Grant-in-Aid for Scientific Research from the Ministry of Education, Culture, Sports, Science and Technology (MEXT), Japan (O. Nagano and H. Saya); the Global COE Program, MEXT, Japan (M. Tamada, M. Ohmura, and M. Suematsu); the Grant-in-Aid for JSPS Fellows DC2 (M. Tamada); and "Next Generation Integrated Simulation of Living Matter" project, part of the Development and Use of the Next-Generation Supercomputer Project of MEXT (M. Ohmura).

The costs of publication of this article were defrayed in part by the payment of page charges. This article must therefore be hereby marked *advertisement* in accordance with 18 U.S.C. Section 1734 solely to indicate this fact.

Received September 8, 2011; revised January 12, 2012; accepted January 26, 2012; published OnlineFirst January 31, 2012.

References

1. Warburg O, Wind F, Negelein E. The metabolism of tumors in the body. J Gen Physiol 1927;8:519–30.
2. Gatenby RA, Gillies RJ. Why do cancers have high aerobic glycolysis? Nat Rev Cancer 2004;4:891–9.
3. Bonnet S, Archer SL, Allalunis-Turner J, Haromy A, Beaulieu C, Thompson R, et al.A mitochondria-K+ channel axis is suppressed in cancer and its normalization promotes apoptosis and inhibits cancer growth. Cancer Cell 2007;11:37–51.
4. Matoba S, Kang JG, Patino WD, Wragg A, Boehm M, Gavrilova O, et al. p53 regulates mitochondrial respiration. Science 2006;312:1650–3.
5. Jiang P, Du W, Wang X, Mancuso A, Gao X, Wu M, et al. p53 regulates biosynthesis through direct inactivation of glucose-6-phosphate dehydrogenase. Nat Cell Biol 2011;13:310–6.
6. Godar S, Ince TA, Bell GW, Feldser D, Donaher JL, Bergh J, et al. Growth-inhibitory and tumor- suppressive functions of p53 depend on its repression of CD44 expression. Cell 2008;134:62–73.
7. Aruffo A, Stamenkovic I, Melnick M, Underhill CB, Seed B. CD44 is the principal cell surface receptor for hyaluronate. Cell 1990;61:1303–13.
8. Ponta H, Sherman L, Herrlich PA. CD44: from adhesion molecules to signalling regulators. Nat Rev Mol Cell Biol 2003;4:33–45.
9. Visvader JE, Lindeman GJ. Cancer stem cells in solid tumours: accumulating evidence and unresolved questions. Nat Rev Cancer 2008;8:755–68.
10. Ishimoto T, Nagano O, Yae T, Tamada M, Motohara T, Oshima H, et al. CD44 variant regulates redox status in cancer cells by stabilizing the xCT subunit of system xc(-) and thereby promotes tumor growth. Cancer Cell 2011;19:387–400.
11. Christofk HR, Vander Heiden MG, Harris MH, Ramanathan A, Gerszten RE, Wei R, et al. The M2 splice isoform of pyruvate kinase is important for cancer metabolism and tumour growth. Nature 2008;452:230–3.
12. Hitosugi T, Kang S, Vander Heiden MG, Chung TW, Elf S, Lythgoe K, et al. Tyrosine phosphorylation inhibits PKM2 to promote the Warburg effect and tumor growth. Sci Signal 2009;2:ra73.
13. Christofk HR, Vander Heiden MG, Wu N, Asara JM, Cantley LC. Pyruvate kinase M2 is a phosphotyrosine-binding protein. Nature 2008;452:181–6.
14. Vander Heiden MG, Locasale JW, Swanson KD, Sharfi H, Heffron GJ, Amador-Noguez D, et al. Evidence for an alternative glycolytic pathway in rapidly proliferating cells. Science 2010;329:1492–9.
15. Tateyama S, Horisawa K, Takashima H, Miyamoto-Sato E, Doi N, Yanagawa H. Affinity selection of DNA-binding protein complexes using mRNA display. Nucleic Acids Res 2006;34:e27.
16. Horisawa K, Tateyama S, Ishizaka M, Matsumura N, Takashima H, Miyamoto-Sato E, et al. *In vitro* selection of Jun-associated proteins using mRNA display. Nucleic Acids Res 2004;32:e169.
17. Miyamoto-Sato E, Ishizaka M, Horisawa K, Tateyama S, Takashima H, Fuse S, et al. Cell-free cotranslation and selection using *in vitro* virus for high-throughput analysis of protein-protein interactions and complexes. Genome Res 2005;15:710–7.
18. Kinoshita A, Tsukada K, Soga T, Hishiki T, Ueno Y, Nakayama Y, et al. Roles of hemoglobin Allostery in hypoxia-induced metabolic alterations in erythrocytes: simulation and its verification by metabolome analysis. J Biol Chem 2007;282:10731–41.
19. Soga T, Baran R, Suematsu M, Ueno Y, Ikeda S, Sakurakawa T, et al. Differential metabolomics reveals ophthalmic acid as an oxidative stress biomarker indicating hepatic glutathione consumption. J Biol Chem 2006;281:16768–76.

Published OnlineFirst on January 31, 2012; DOI:10.1158/0008-5472.CAN-11-3024

20. Kawauchi K, Araki K, Tobiume K, Tanaka N. p53 regulates glucose metabolism through an IKK-NF-kappaB pathway and inhibits cell transformation. Nat Cell Biol 2008;10:611–8.
21. Arima Y, Nitta M, Kuninaka S, Zhang D, Fujiwara T, Taya Y, et al. Transcriptional blockade induces p53-dependent apoptosis associated with translocation of p53 to mitochondria. J Biol Chem 2005;280:19166–76.
22. Sudo T, Nitta M, Saya H, Ueno NT. Dependence of paclitaxel sensitivity on a functional spindle assembly checkpoint. Cancer Res 2004;64:2502–8.
23. Furuta E, Okuda H, Kobayashi A, Watabe K. Metabolic genes in cancer: their roles in tumor progression and clinical implications. Biochim Biophys Acta 2010;1805:141–52.
24. Ganapathy V, Thangaraju M, Prasad PD. Nutrient transporters in cancer: relevance to Warburg hypothesis and beyond. Pharmacol Ther 2009;121:29–40.
25. Hamrahian AH, Zhang JZ, Elkhairi FS, Prasad R, Ismail-Beigi F. Activation of Glut1 glucose transporter in response to inhibition of oxidative phosphorylation. Arch Biochem Biophys 1999;368:375–9.
26. Ebert BL, Firth JD, Ratcliffe PJ. Hypoxia and mitochondrial inhibitors regulate expression of glucose transporter-1 via distinct Cis-acting sequences. J Biol Chem 1995;270:29083–9.
27. Okamoto I, Tsuiki H, Kenyon LC, Godwin AK, Emlet DR, Holgado-Madruga M, et al. Proteolytic cleavage of the CD44 adhesion molecule in multiple human tumors. Am J Pathol 2002;160:441–7.
28. Xu RH, Pelicano H, Zhou Y, Carew JS, Feng L, Bhalla KN, et al. Inhibition of glycolysis in cancer cells: a novel strategy to overcome drug resistance associated with mitochondrial respiratory defect and hypoxia. Cancer Res 2005;65:613–21.
29. Bragado P, Armesilla A, Silva A, Porras A. Apoptosis by cisplatin requires p53 mediated p38alpha MAPK activation through ROS generation. Apoptosis 2007;12:1733–42.
30. Teicher BA. Hypoxia and drug resistance. Cancer Metastasis Rev 1994;13:139–68.
31. Song X, Liu X, Chi W, Liu Y, Wei L, Wang X, et al. Hypoxia-induced resistance to cisplatin and doxorubicin in non-small cell lung cancer is inhibited by silencing of HIF-1alpha gene. Cancer Chemother Pharmacol 2006;58:776–84.
32. Schafer ZT, Grassian AR, Song L, Jiang Z, Gerhart-Hines Z, Irie HY, et al. Antioxidant and oncogene rescue of metabolic defects caused by loss of matrix attachment. Nature 2009;461:109–13.
33. Gottlieb E. Cancer: the fat and the furious. Nature 2009;461:44–5.
34. Rahman I, Kode A, Biswas SK. Assay for quantitative determination of glutathione and glutathione disulfide levels using enzymatic recycling method. Nat Protoc 2006;1:3159–65.
35. Dallas NA, Xia L, Fan F, Gray MJ, Gaur P, van Buren G II, et al. Chemoresistant colorectal cancer cells, the cancer stem cell phenotype, and increased sensitivity to insulin-like growth factor-I receptor inhibition. Cancer Res 2009;69:1951–7.
36. Phillips TM, McBride WH, Pajonk F. The response of CD24(-/low)/CD44 +breast cancer-initiating cells to radiation. J Natl Cancer Inst 2006;98:1777–85.
37. Choi KJ, Piao YJ, Lim MJ, Kim JH, Ha J, Choe W, et al. Overexpressed cyclophilin A in cancer cells renders resistance to hypoxia- and cisplatin-induced cell death. Cancer Res 2007;67:3654–62.
38. Hwang IT, Chung YM, Kim JJ, Chung JS, Kim BS, Kim HJ, et al. Drug resistance to 5-FU linked to reactive oxygen species modulator 1. Biochem Biophys Res Commun 2007;359:304–10.
39. Aluise CD, St Clair D, Vore M, Butterfield DA. *In vivo* amelioration of adriamycin induced oxidative stress in plasma by gamma-glutamylcysteine ethyl ester (GCEE). Cancer Lett 2009;282:25–9.
40. Siddik ZH. Cisplatin: mode of cytotoxic action and molecular basis of resistance. Oncogene 2003;22:7265–79.
41. Lowe SW, Ruley HE, Jacks T, Housman DE. p53-dependent apoptosis modulates the cytotoxicity of anticancer agents. Cell 1993;74:957–67.
42. Liu L, Sun L, Zhang H, Li Z, Ning X, Shi Y, et al. Hypoxia-mediated up-regulation of MGr1-Ag/37LRP in gastric cancers occurs via hypoxia-inducible-factor 1-dependent mechanism and contributes to drug resistance. Int J Cancer 2009;124:1707–15.

nature COMMUNICATIONS

ARTICLE

Received 6 Jan 2012 | Accepted 8 May 2012 | Published 6 Jun 2012

DOI: 10.1038/ncomms1892

Alternative splicing of *CD44* mRNA by ESRP1 enhances lung colonization of metastatic cancer cell

Toshifumi Yae[1,2], Kenji Tsuchihashi[1], Takatsugu Ishimoto[1], Takeshi Motohara[1], Momoko Yoshikawa[1], Go J. Yoshida[1], Takeyuki Wada[1], Takashi Masuko[3], Kaoru Mogushi[4], Hiroshi Tanaka[4], Tsuyoshi Osawa[5], Yasuharu Kanki[5], Takashi Minami[5], Hiroyuki Aburatani[6], Mitsuyo Ohmura[7], Akiko Kubo[7], Makoto Suematsu[7,8], Kazuhisa Takahashi[2], Hideyuki Saya[1,9] & Osamu Nagano[1]

In cancer metastasis, various environmental stressors attack the disseminating cells. The successful colonization of cancer cells in secondary sites therefore requires the ability of the cells to avoid the consequences of such exposure to the stressors. Here we show that orthotopic transplantation of a CD44 variant isoform-expressing ($CD44v^+$) subpopulation of 4T1 breast cancer cells, but not that of a $CD44v^-$ subpopulation, in mice results in efficient lung metastasis accompanied by expansion of stem-like cancer cells. Such metastasis is dependent on the activity of the cystine transporter xCT, and the stability of this protein is controlled by CD44v. We find that epithelial splicing regulatory protein 1 regulates the expression of CD44v, and knockdown of epithelial splicing regulatory protein 1 in $CD44v^+$ cells results in an isoform switch from CD44v to CD44 standard (CD44s), leading to reduced cell surface expression of xCT and suppression of lung colonization. The epithelial splicing regulatory protein 1-CD44v-xCT axis is thus a potential therapeutic target for the prevention of metastasis.

[1] Division of Gene Regulation, Institute for Advanced Medical Research, School of Medicine, Keio University, 35 Shinanomachi, Shinjuku-ku, Tokyo 160-8582, Japan. [2] Department of Respiratory Medicine, Juntendo University, School of Medicine, 2-1-1 Hongo, Bunkyo-Ku, Tokyo 113-8421, Japan. [3] Cell Biology Laboratory, Department of Pharmaceutical Sciences, School of Pharmacy, Kinki University, 4-1 Kowakae 3-chome, Higashiosaka-shi, Osaka 577-8502, Japan. [4] Department of Bioinformatics, Division of Medical Genomics, Medical Research Institute, Tokyo Medical and Dental University 1-5-45 Yushima, Bunkyo-Ku, Tokyo 113-8510, Japan. [5] Lab for Vascular Biology, RCAST, The University of Tokyo, 4-6-1 Komaba, Meguro-ku, Tokyo 153-8904, Japan. [6] Genome Science Division, RCAST, The University of Tokyo, 4-6-1 Komaba, Meguro-ku, Tokyo 153-8904, Japan. [7] Department of Biochemistry, School of Medicine, Keio University, 35 Shinanomachi, Shinjuku-ku, Tokyo 160-8582, Japan. [8] Japan Science and Technology Agency, Exploratory Research for Advanced Technology (ERATO), Suematsu Gas Biology Project, Tokyo 102-0076, Japan. [9] Japan Science and Technology Agency, Core Research for Evolutional Science and Technology (CREST), Tokyo 102-0076, Japan. Correspondence and requests for materials should be addressed to O.N. (email: osmna@sb3.so-net.ne.jp) or to H.S. (email: hsaya@a5.keio.jp).

Metastasis is the major cause of death for individuals with solid tumours[1], largely because of the ineffectiveness of current therapies, once metastasis is established[2,3]. Metastasis is an inefficient process, however, with few cells released from a primary tumour eventually reinitiating tumour growth at distant sites. The formation of metastases has therefore been thought to result from the dissemination of stem-like cancer cells and their colonization of secondary sites[4,5]. The cell surface protein CD44 is a major marker for stem-like cancer cells[6–9] and is also highly expressed in metastatic cancer cells[4,6]. Although differences in CD44$^+$ stem-like cells between primary tumours and metastases remain ill-defined, a subset of CD44$^+$ stem-like cells in primary tumours might possess the ability to reinitiate tumour growth at distant sites[4,6]. It has remained largely unknown, however, whether CD44 is functionally associated with metastatic propagation by stem-like cancer cells.

CD44 has been implicated in a variety of physiological processes in addition to cancer cell invasion and metastasis[10–13]. CD44 exists in numerous isoforms generated through alternative messenger RNA splicing[14], with variability in the extracellular domain of CD44 being thought to underlie the functional diversity of this molecule[13,15]. A CD44 variant (CD44v) isoform containing v3 (the sequence encoded by variant exon 3) that undergoes heparin sulphate modification has thus been shown to interact with various growth factors including heparin-binding epidermal growth factor-like growth factor and basic fibroblast growth factor[16], whereas the CD44v6 isoform has been shown to act as a co-receptor for the receptor tyrosine kinase c-Met[17]. Furthermore, we recently showed that interaction of CD44v8-10 with the cystine transporter xCT (SLC7A11) stabilizes the latter protein and thereby potentiates the ability of cancer cells to defend themselves against reactive oxygen species (ROS)[18]. The generation of CD44v isoforms might therefore modulate the activity of various plasma membrane proteins including receptor tyrosine kinases and transporters in cancer cells.

Given that cancer cells are exposed to environmental stressors such as oxygen or nutrient deficiency, low pH, inflammatory mediators, and ROS during metastasis, the ability to avoid the consequences of such exposure is required for successful colonization by cancer cells[19–21]. The cystine transporter xCT functions as a Na^+-independent transporter that mediates the exchange of extracellular cystine for intracellular glutamate and thereby promotes the synthesis of reduced glutathione (GSH)[22,23], a ubiquitous reducing thiol peptide that serves as an important intracellular redox buffer and is associated with resistance of cancer cells to anticancer agents[24,25]. The availability of cysteine is rate-limiting for GSH synthesis[26], and the activity of xCT is therefore essential for such resistance to anticancer agents[23,27]. However, the functional relevance of CD44v and xCT in the metastatic spread of stem-like cancer cells has remained undetermined. Here we show that CD44v–xCT expression regulated by ESRP1 in metastatic breast cancer cells confers the ability of evasion from oxidative stress and thereby promotes the lung metastasis. These findings suggest that CD44v may be a therapeutic target.

Results

Metastatic subpopulation in 4T1 cells expresses CD44v. To investigate the role of CD44v in cancer metastasis, we studied the mouse breast cancer cell line 4T1 and its isogenic sublines (4T07, 168FARN, 67NR). All of these cells form primary tumours in mice, but only 4T1 cells give rise to visible lung metastases[28] (Fig. 1a). RT–PCR analysis revealed that the abundance of CD44v messenger RNA was markedly greater than that of CD44s mRNA in 4T1 cells, whereas only CD44s mRNA was detected in the nonmetastatic sublines (Fig. 1b; Supplementary Fig. S1). Flow cytometry showed that 4T1 cells consist of two subpopulations, CD44v$^+$ cells (which predominantly express CD44v) and CD44v$^-$ cells (which express only CD44s), whereas the nonmetastatic sublines consist only of CD44v$^-$ cells (Fig. 1c), suggesting that CD44v might be associated with the metastatic ability of 4T1 cells. We isolated the CD44v$^+$ and CD44v$^-$ subpopulations of 4T1 cells by fluorescence-activated cell sorting (FACS) and subjected these cells to immunoblot analysis and to analysis followed by direct sequencing of the PCR products[29] (Supplementary Fig. S1 and Supplementary Methods). The predominant CD44v isoform in the CD44v$^+$ cells was found to be CD44v8-10. Each subpopulation was transplanted (1×10^5 cells) into mouse mammary glands. The incidence (CD44v$^+$, 13/13; CD44v$^-$, 11/11) and volume (Fig. 1d) of the primary tumours derived from CD44v$^+$ or CD44v$^-$ cells were similar. However, the incidence of lung metastasis by CD44v$^+$ cells was markedly higher than that of CD44v$^-$ cells (CD44v$^+$, 13/13; CD44v$^-$, 3/11), and both IntegriSense quantitative fluorescence imaging[30] and histological analysis revealed that the extent of lung metastatic lesions derived from CD44v$^+$ cells was greater than that of those formed by CD44v$^-$ cells (Fig. 1e,f). The CD44v$^+$ subpopulation was thus enriched in highly metastatic cells compared with the CD44v$^-$ subpopulation.

Given that 4T1 cells are resistant to 6-thioguanine (6-TG)[28], we isolated tumour cells by 6-TG selection from lung metastases formed after injection of CD44v$^-$ cells into the tail vein. Small metastatic nodules consisted mostly of CD44v$^-$ cells, suggesting that CD44v$^-$ cells also possess metastasis-initiating ability (Fig. 1g). However, when CD44v$^+$ and CD44v$^-$ cells were injected at a 50:50 ratio, lung metastases consisted mostly of CD44v$^+$ cells (Fig. 1g), indicating that the lung colonization potential of CD44v$^+$ cells is much higher than that of CD44v$^-$ cells.

ESRP1 promotes lung metastasis of 4T1 cells. To identify the mechanism underlying lung colonization potential, we performed microarray analysis (Supplementary Methods) followed by gene set enrichment analysis (GSEA)[31]. The CD44v$^+$ cell/CD44v$^-$ cell gene set profile was similar to the embryonic stem (ES) cell/mouse embryonic fibroblast (MEF) and induced pluripotent stem (iPS) cell/MEF profiles (Fig. 2a). CD44v$^+$ cells thus manifest an ES cell-like gene signature when compared with CD44v$^-$ cells. The gene for epithelial splicing regulatory protein 1 (ESRP1), which regulates alternative splicing of CD44 mRNA[14], was highly expressed not only in CD44v$^+$ 4T1 cells but also in ES and iPS cells (Supplementary Data 1). We therefore examined the role of this protein in metastasis. An ES cell-like gene expression signature has been associated with an aggressive phenotype in cancer[32], and so we examined the relation between *ESRP1* expression and prognosis with the use of gene expression profiles of breast cancer patients[33]. A high level of *ESRP1* expression was significantly associated with a lower rate of overall survival (Fig. 2b), suggesting that increased ESRP1 expression is related to the malignant behaviour of human breast cancer.

The abundance of ESRP1 mRNA was significantly higher in CD44v$^+$ 4T1 cells than in CD44v$^-$ 4T1 cells and 67NR cells (Fig. 2c), suggesting that ESRP1 regulates CD44v expression. We established CD44v$^+$ 4T1 cells that stably express either a short hairpin RNA (shRNA) specific for ESRP1 mRNA (shESRP1 CD44v$^+$ cells) or a corresponding scrambled (control) shRNA (shC CD44v$^+$ cells) (Supplementary Methods). ESRP1 knockdown resulted in a switch in CD44 mRNA splicing that led to the generation of the CD44 standard isoform (CD44s) mRNA rather than CD44v mRNA (Fig. 2d). Furthermore, the mRNAs for Mena, fibroblast growth factor receptor 2 (FGFR2), and p120 catenin, whose splicing is also regulated by ESRP1 (ref. 14), underwent a shift in splicing pattern in shESRP1 CD44v$^+$ cells (Fig. 2d). Flow cytometry also revealed that ESRP1 depletion resulted in a pronounced conversion from the production of CD44v to that of CD44s without an effect on the overall level of CD44 expression (Fig. 2e). To determine whether ESRP1 contributes to the metastatic behaviour of CD44v$^+$ cells, we transplanted shC CD44v$^+$ or shESRP1 CD44v$^+$ cells orthotopically into mouse mammary glands. Although the incidence (shC CD44v$^+$,